Relaxing cosmological tensions with a sign switching cosmological constant: Improved results with Planck, BAO, and Pantheon data

Özgür Akarsu,[1,*] Suresh Kumar,[2,†] Emre Özülker,[1,‡] J. Alberto Vazquez,[3,§] and Anita Yadav[2,‖]

[1]*Department of Physics, Istanbul Technical University, Maslak, 34469 Istanbul, Turkey*
[2]*Department of Mathematics, Indira Gandhi University, Meerpur, Haryana-122502, India*
[3]*Instituto de Ciencias Físicas, Universidad Nacional Autónoma de México, Cuernavaca, Morelos 62210, Mexico*

(Received 13 November 2022; accepted 9 June 2023; published 14 July 2023)

We present a further observational analysis of the Λ_sCDM model proposed in Akarsu *et al.* [Phys. Rev. D **104**, 123512 (2021)]. This model is based on the recent conjecture suggesting the Universe has transitioned from anti–de Sitter vacua to de Sitter vacua (viz., the cosmological constant switches sign from negative to positive), at redshift $z_\dagger \sim 2$, inspired by the graduated dark energy model proposed in Akarsu *et al.* [Phys. Rev. D **101**, 063528 (2020)]. Λ_sCDM was previously claimed to simultaneously relax five cosmological discrepancies, namely, the H_0, S_8, and M_B tensions along with the Ly-α and ω_b anomalies, which prevail within the standard ΛCDM model as well as its canonical/simple extensions. In the present work, we extend the previous analysis by constraining the model using the Pantheon data (with and without the SH0ES M_B prior) and/or the *completed* BAO data along with the full *Planck* CMB data. We find that Λ_sCDM exhibits a better fit to the data compared to ΛCDM, and simultaneously relaxes the six discrepancies of ΛCDM, viz., the H_0, M_B, S_8, Ly-α, t_0, and ω_b discrepancies, all of which are discussed in detail. When the M_B prior is included in the analyses, Λ_sCDM performs significantly better in relaxing the H_0, M_B, and S_8 tensions with the constraint $z_\dagger \sim 1.8$ even when the Ly-α data (which imposed the $z_\dagger \sim 2$ constraint in the previous studies) are excluded. In contrast, the presence of the M_B prior causes only negligible improvements for ΛCDM. Thus, the Λ_sCDM model provides remedy to various cosmological tensions simultaneously, only that the galaxy BAO data hinder its success to some extent.

DOI: 10.1103/PhysRevD.108.023513

I. INTRODUCTION

In the past decade, there has been a growing consensus that today's standard model of cosmology, namely, the Lambda Cold Dark Matter (ΛCDM) model, is actually an approximation to a more realistic new cosmological model which is yet to be understood. This new model, which may be conceptually very different, is expected to show slight but probably nontrivial phenomenological deviations from ΛCDM, because, despite being in very good agreement with a wide range of astrophysical and cosmological data [1–8], ΛCDM leads to discordances between various cosmological probes increased in diversity and precision over the past decade, e.g., the H_0 and S_8 tensions, and other statistically less significant anomalies [9–17]. While these discordances can still be in part the result of systematic errors, the fact that they survived (and in some cases are even exacerbated) after several years of accurate analyses, points to cracks in ΛCDM, and suggests searching for new physics beyond the well-established fundamental theories that underpin, and even extend, the ΛCDM model. In particular, the H_0 (Hubble constant) tension exceeds 5σ with the recent SH0ES measurement [18] which led it to be called a crisis by many. Moreover, these tensions have turned out to be more challenging than originally thought. For instance, the H_0 tension worsens when the cosmological constant (Λ) is replaced by generic quintessence models of dark energy (DE), and is only partially relaxed when replaced by the simplest phantom (or quintom) models, and troublingly, many of the compelling models that suggest an amelioration in the H_0 tension—such as early dark energy (EDE) [19–22], new-EDE [23,24], and nonminimally interacting dark energy (IDE) [25–28]—result in worsening of others, e.g., the S_8 (weighted amplitude of matter fluctuations) tension, and they can even exacerbate less important anomalies to significant levels [29–37] (see also Refs. [9–17]). One may see Refs. [38–51] suggesting solutions to S_8 tension, some of which suggest relaxing the H_0 tension as well. We refer the reader to Refs. [9–17] for a comprehensive list of references and recent reviews on the cosmological tensions, including

*akarsuo@itu.edu.tr
†suresh.math@igu.ac.in
‡ozulker17@itu.edu.tr
§javazquez@icf.unam.mx
‖anita.math.rs@igu.ac.in

discussions on the cosmological model-independent estimations of parameters such as H_0 and S_8, and a summary of proposed solutions.

It has been reported that the H_0 tension—as well as a number of other discrepancies—could be alleviated by a dynamical DE (as an effective or actual source) that achieves negative (could be persistent or temporary) or rapidly vanishing energy density values in the near or far past; and, this has recently increased interest in the phenomenological and theoretical realization/investigation of such models, see Refs. [52–106]. In fact, the simplest example of this type of scenario is the spatially closed ΛCDM model; positive spatial curvature (analogous to cosmic strings with negative energy density[1]) and positive cosmological constant together can be interpreted as a single effective source that attains negative energy densities in the past and this scenario is significantly preferred over spatially flat ΛCDM by CMB data alone [3]—this preference that can be referred as the curvature, Ω_k, anomaly [107–116], is closely related to the lensing amplitude, $A_{\rm L}$, anomaly [31,107,117] since these two parameters are degenerate. However, the fact that this scenario (also its canonical/simple extensions) worsens the H_0 and S_8 tensions and is no more preferred when the CMB data is combined with other astrophysical data [3,31,85,107–117], may be signaling the need for a source of negative energy density that contributes more unexpectedly to the evolution of the Universe. In particular, it was recently conjectured in Ref. [68] that the Universe underwent a rapid anti–de Sitter (AdS) to de Sitter (dS) vacua transition at redshift $z \sim 2$. This conjecture was based on the fact that observational analyses of the graduated dark energy (gDE) favored its sign-switching cosmological constantlike ($\Lambda_{\rm s}$-like) behavior, and this behavior simultaneously ameliorated the H_0 and Ly-α (Lyman-α) discrepancies; the conjecture was further motivated by some theoretical advantages of $\Lambda_{\rm s}$ over gDE's $\Lambda_{\rm s}$-like behavior. In a later paper [89], the $\Lambda_{\rm s}$CDM model (which simply replaces the usual positive cosmological constant of ΛCDM with $\Lambda_{\rm s}$) was studied in detail in the context of cosmological tensions. In particular, it was explained how this model can simultaneously address the H_0, M_B [Type Ia supernovae (SNIa) absolute magnitude, closely related to the H_0 measurements], and Ly-α discrepancies, and, its observational analyses using the full Planck cosmic microwave background (CMB) and baryon acoustic oscillation (BAO) data were carried out. It was found that $\Lambda_{\rm s}$CDM is able to ameliorate the H_0, M_B, and S_8 tensions along with the Ly-α and $\omega_{\rm b}$ (physical baryon density) anomalies.

In this paper, we expand the investigations in Ref. [89], extend the observational analyses, by using the *completed* BAO data and the Pantheon SNIa sample (with and without an M_B prior) along with the full Planck CMB data, extend the previous discussions on the H_0, M_B, S_8, Ly-α, and $\omega_{\rm b}$ discrepancies within $\Lambda_{\rm s}$CDM, and further add the t_0 (present-day age of the Universe) discrepancy and a theoretical explanation of how the S_8 tension can be alleviated in this model. In Sec. II, we briefly present the $\Lambda_{\rm s}$CDM model and motivate it starting from the gDE and by discussing its behavior with respect to tensions of ΛCDM. In Sec. III, we first present the methodology and data sets used in the observational analyses and then discuss the results. In Sec. IV, we briefly explain six discrepancies of ΛCDM, viz., the H_0, M_B, S_8, Ly-α, t_0, and $\omega_{\rm b}$, and assess their situation within $\Lambda_{\rm s}$CDM for our data sets, and we conclude in Sec. V.

II. THE $\Lambda_{\rm s}$CDM MODEL

The standard ΛCDM model relies on the presence of a constant energy density term, Λ—such as the usual vacuum energy of QFT and/or an effective energy density of a geometrical cosmological constant—to drive the present-day acceleration of the Universe; this constant energy density corresponds to zero inertial mass density $\varrho = 0$, where $\varrho \equiv \rho + p$ with ρ and p being energy density and pressure, respectively. A minimal dynamical deviation from the zero inertial mass density assumption in the form of $\varrho \propto \rho^{\lambda}$, called graduated dark energy, was first investigated in Ref. [68]. Having almost constant negative energy density values at large redshifts, gDE settles into a positive value in the late Universe after a continuous transition whose rapidity is controlled by the parameter λ. During the transition, its energy density vanishes at a redshift, $z_\dagger$, and exhibits a pole in its equation of state (EoS) parameter that is characteristic of the DE models with sign-changing density [96]. The parameter space of the gDE was well-constrained in its observational analysis (see Ref. [68]) with a preference of $z_\dagger \approx 2.3$ and large negative values of λ, in which case the gDE resembles (becomes exact for $\lambda \to -\infty$) a negative cosmological constant, $\Lambda_- < 0$, that instantaneously switches sign at $z \approx 2.3$ and attains its present-day positive value $\Lambda_+ = |\Lambda_-|$. Compared to the usual cosmological constant, the gDE shows better agreement with multitude of data. In particular, when analysed with a combined data set from CMB, BAO, SNIa, and cosmic chronometers (CCs), the gDE model had a significantly better fit with a nonmonotonic behavior of $H(z)$ around $z_\dagger \approx 2.3$ that allowed the model to bring Ly-α BAO (BOSS DR11) data [53] in concordance with the rest of the

[1]They are analogous in the sense that both contribute to the Friedmann equation as a negative energy source with an equation of state parameter equal to $-1/3$. However, the presence of spatial curvature also has the effect of modifying the interrelations of cosmological distance measures (e.g., the comoving angular diameter distance is no longer proportional to the line-of-sight comoving distance for nonzero spatial curvature), rendering these two scenarios quite different. A similar distinction also arises when considering the combination of Λ and spatial curvature as a single effective source in the Friedmann equation.

observations. Moreover, it yielded a value of $H_0 = 69.7 \pm 0.9\ \mathrm{km\,s^{-1}\,Mpc^{-1}}$ which is in perfect agreement with the local $H_0 = 69.8 \pm 0.8\ \mathrm{km\,s^{-1}\,Mpc^{-1}}$ measurement from the tip of the red giant branch (TRGB) [118]. In the gDE framework, these two simultaneous improvements in H_0 and Ly-α are interrelated in the following sense. A $z_\dagger$ value smaller than the effective redshift of the Ly-α data leads the model to have negative DE density at that effective redshift and beyond (towards early universe). Such a negative DE is in line with the lesser $H(z)$ value of the Ly-α data (less than the prediction of ΛCDM when constrained by the CMB). And since the comoving angular diameter distance to last scattering, $D_M(z_*)$, which is directly related to the integral of $H^{-1}(z)$, is strictly constrained by observations almost model independently, the lesser value of $H(z)$ at the effective redshift of the Ly-α data should be compensated by a higher $H(z)$ value somewhere else, which, for the gDE, results in a higher H_0 value [68] (see also Refs. [89,100], for a detailed discussion).

Inspired by the observational findings, and the fact that a sign-switching cosmological constant corresponding to the $\lambda \to -\infty$ limit of the gDE, unlike gDE with a finite λ, evades violating the weak energy condition and bounds on the speed of sound, the authors conjectured in Ref. [68] that the cosmological constant has spontaneously switched sign, i.e., the Universe has transitioned from AdS vacuum with Λ_- to dS vacuum with Λ_+. The simplest sign-switching cosmological constant model, Λ_sCDM, can be phenomenologically constructed by promoting the usual cosmological constant (Λ) of the standard ΛCDM model to an abruptly sign-switching (switches at a redshift $z_\dagger$ which is the only extra free parameter on top of the standard ΛCDM) cosmological constant (Λ_s) with a present-day value of $\Lambda_{\mathrm{s}0} > 0$, i.e.,

$$\Lambda \to \Lambda_\mathrm{s} \equiv \Lambda_{\mathrm{s}0}\,\mathrm{sgn}[z_\dagger - z], \tag{1}$$

where, the sign-switch feature is realized by the signum function, "sgn", that reads $\mathrm{sgn}[x] = -1,\ 0,\ 1$ for $x < 0$, $x = 0$ and $x > 0$, respectively [89]. Before moving on to the cosmological implications of the Λ_sCDM model in the light of observational data, it may be helpful to comment on a few subtleties to gain a clear understanding of this model. The sign-switching transition of Λ_s described here by the signum function (implying an abrupt transition) should be understood as an idealized description of a rapid transition (may or may not be smooth) from an AdS vacuum provided by $\Lambda_\mathrm{s} = -\Lambda_{\mathrm{s}0}$ to a dS vacuum provided by $\Lambda_\mathrm{s} = \Lambda_{\mathrm{s}0}$, or DE models such as gDE, that can mimic this behavior. Such transitions that are also smooth, can easily be constructed/described phenomenologically using sigmoid functions, e.g., the hyperbolic tangent, $\tanh[x]$, and the logistic function, $1/(1+e^{-x})$. Accordingly, one can replace Eq. (1) with, for example, $\Lambda_\mathrm{s} \equiv \Lambda_{\mathrm{s}0}\tanh[\eta(z_\dagger - z)]$ which comes with two extra free parameters on top of ΛCDM, namely, η and $z_\dagger$.[2] Of these two, $\eta > 0$ determines the rapidity of the transition from $-\Lambda_{\mathrm{s}0}$ to $\Lambda_{\mathrm{s}0}$ around $z = z_\dagger$ and the limit $\eta \to +\infty$ leads to the abrupt sign-switch behavior considered in Eq. (1). In Λ_sCDM, we simply replace the Λ of ΛCDM with Λ_s, so that all material constituents of the Universe are locally conserved separately, and thus Λ_s also submits to the usual continuity equation due to the twice-contracted Bianchi identity in general relativity (GR). Accordingly, the corresponding EoS parameter reads $w_{\Lambda_\mathrm{s}} = -1 - \eta(1+z)(1-\tanh^2[\eta(z_\dagger - z)])/3\tanh[\eta(z_\dagger - z)]$, which exhibits a pole at $z = z_\dagger$ (viz., yields $\lim_{z\to z_\dagger^\pm} w_{\Lambda_\mathrm{s}}(z) = \pm\infty$; such a singularity[3] is necessary for the energy density to change sign [96]) and, approaching minus unity more and more with increasing $|z_\dagger - z|$, becomes indistinguishable from $w_{\Lambda_\mathrm{s}} = -1$ for all redshifts far enough away from $z_\dagger$. We note that for a given definition of Λ_s, the corresponding EoS parameter w_{Λ_s} is free to behave as necessary to ensure that the Λ_s satisfies the continuity equation, and when the limit $\eta \to +\infty$ corresponding to the abrupt sign-switch behavior in Eq. (1) is taken at face value, $w_{\Lambda_\mathrm{s}}(z \neq z_\dagger) = -1$ would be satisfied and the deviation of w_{Λ_s} from minus unity would be squeezed into the single redshift[4] $z = z_\dagger$; see Sec. V for more comments on the abrupt sign-switch scenario and potential mechanisms underlying it. On the other hand, from a phenomenological point of view, for sufficiently large values of η, the $\mathrm{sgn}[x]$ and $\tanh[x]$ parametrizations become barely distinguishable; however, working with the abrupt AdS-dS transition as defined in Eq. (1) is much more convenient thanks to its simplicity, particularly for observational analyses. For instance, for $\eta = 100$, we have $|\Lambda_\mathrm{s}| = \Lambda_{\mathrm{s}0}$ with 10^{-2} percent

[2]Another Λ_s, extending the usual Λ with two extra parameters $(z_\dagger, \gamma)$, can be defined: $\Lambda_\mathrm{s} \equiv \Lambda_{\mathrm{s}0}(\gamma\,\mathrm{sgn}[z_\dagger - z] - \gamma + 1)$, in which case the new parameter $\gamma > 1/2$ determines the depth of the AdS vacuum, $\Lambda_- = \Lambda_{\mathrm{s}0}(1-2\gamma)$. Further, once again sgn function can be replaced with continuous sigmoid functions, e.g., $\Lambda_\mathrm{s} \equiv \Lambda_{\mathrm{s}0}(\gamma\tanh[\eta(z_\dagger - z) + \mathrm{arctanh}[1-1/\gamma]] - \gamma + 1)$ defines a Λ_s with three extra parameters $(z_\dagger, \eta, \gamma)$ that smoothly transitions from $\Lambda_- = \Lambda_{\mathrm{s}0}(1-2\gamma)$ to $\Lambda_+ = \Lambda_{\mathrm{s}0}$ with a rapidity controlled by $\eta > 0$, and vanishes at $z = z_\dagger$.

[3]For some examples with EoS parameters presenting singularities of the same type, see Refs. [54,55,60,64,65,68,85,91,100,104,106] where they are studied within the context of cosmological tensions; and see Refs. [119–123] for some earlier examples.

[4]Discontinuity of the signum function results in mild complications in familiar notions, e.g., the spacetime metric is no longer differentiable at $z = z_\dagger$ (though, it is continuous; see the solution of the metric for Λ_sCDM in Ref. [89]) and imposing that the Λ_s is conserved requires making use of generalized functions (distributions) to express its corresponding EoS parameter. We do not concern ourselves with such mathematical intricacies in the present study because the discontinuous Λ_s as defined in Eq. (1) can be treated as an idealized parametrization/limiting case as stated in the main text.

precision and $w_{\Lambda_s} = -1$ with one percent precision at $z = z_\dagger \pm 0.05$, improving to 10^{-6} percent precision and 10^{-4} percent precision, respectively, at $z = z_\dagger \pm 0.1$. Thus, the abrupt sign-switching Λ_s we consider in this study can also be taken as an approximation for the more general, but rapidly sign-switching Λ_s models using, for instance, continuous sigmoid functions.

In Ref. [89], Λ_sCDM was analyzed both theoretically and observationally; when the consistency of the model with the CMB is ensured, (i) H_0 and M_B values are inversely correlated with $z_\dagger$ and reach $H_0 \approx 73.4$ km s^{-1} Mpc^{-1} and $M_B \approx -19.25$ mag for $z_\dagger = 1.6$ in remarkable agreement with the measurements from SH0ES [18,124], and (ii) the model inherently presents an excellent fit to the Ly-α data provided that $z_\dagger \lesssim 2.34$. Since Λ_sCDM is equivalent to ΛCDM for $z < z_\dagger$ except for the values of its parameters, it respects the internal consistency of the methodology used by local H_0 measurements that infer it from M_B by assuming a ΛCDM-like cosmography [118,125] such as SH0ES and TRGB; thus, resolving the H_0 tension within Λ_sCDM is almost equivalent to resolving the M_B tension [89]. To see if the model can achieve these promising features, it was confronted with observational data in Ref. [89]; when only the CMB data set from *Planck* 2018 is used, the model yields to $H_0 = 70.22 \pm 1.78$ km s^{-1} Mpc^{-1} with weak constraints on $z_\dagger$, and when BAO are also included with the CMB data set, it yields to $H_0 = 68.82 \pm 0.55$ km s^{-1} Mpc^{-1}, fully consistent with the TRGB measurement $H_0 = 69.8 \pm 0.8$ km s^{-1} Mpc^{-1} [118] (or $H_0 = 69.8 \pm 0.6$ km s^{-1} Mpc^{-1} [126]), and a well-constrained $z_\dagger = 2.44 \pm 0.29$, removing the $\sim 2\sigma$ discrepancy with the Ly-α DR14 [127] measurements that arises within ΛCDM. The lower and upper limits of $z_\dagger$ are controlled by the Galaxy and Ly-α BAO data, respectively, and the larger $z_\dagger$ values imposed by the Galaxy BAO data prevent the model from agreeing perfectly with the SH0ES measurements of $H_0 = 73.04 \pm 1.04$ km s^{-1} Mpc^{-1} [18] and $M_B = -19.244 \pm 0.037$ mag [124]. Furthermore, the observational analyses of Ref. [89] show that lower values of $z_\dagger$ also alleviate the S_8 tension despite having larger σ_8 (amplitude of mass fluctuations on scales of $8h^{-1}$ Mpc with $h \equiv H_0/100$ km s^{-1} Mpc^{-1} being the dimensionless reduced Hubble constant), i.e., more structures, and also in the case of CMB + BAO data, Λ_sCDM accommodates a physical baryon density lower than that of ΛCDM in better agreement with its recent estimations from BBN constraints on the abundance of light elements such as $100\omega_b = 2.233 \pm 0.036$ [128]. In summary, as $z_\dagger$ gets smaller, four discrepancies of ΛCDM, viz., the H_0, M_B, S_8, and Ly-α discrepancies, are better alleviated with potential improvements in the ω_b discrepancy; and for $z_\dagger \sim 1.6$ which is not preferred by the Galaxy BAO data, Λ_sCDM can have remarkable agreement with multitude of observational data including the above four that ΛCDM is discordant with.

Besides all these superior phenomenological aspects of Λ_sCDM over ΛCDM, Λ_sCDM is also one of the simplest one-parameter extensions of ΛCDM. In fact, it is identical to ΛCDM for both $z < z_\dagger$ and $z > z_\dagger$ except for the values of its parameters, in the sense that the Friedmann equations restricted to either one of these intervals have the same functional form; for other equivalently simple models inspired by Λ_sCDM, see Ref. [129]. Thus, it is highly tempting to further explore how Λ_sCDM is a good candidate to replace ΛCDM by extending the work of Ref. [89] both theoretically and observationally. In Ref. [89], a detailed discussion was given on how it can alleviate the discrepancies with H_0, M_B, and BAO Ly-α measurements, and how these discrepancies are affected by the extra free parameter $z_\dagger$; in the observational analyses, CMB alone was found to be consistent with any value of $z_\dagger \gtrsim 1.5$, and it was constrained to $z_\dagger \gtrsim 2.3$ when the BAO data was included in the analysis. In what follows, we first expand the observational analysis of Ref. [89], by using the CMB data combined with the Pantheon data (with and without the M_B prior from the SH0ES measurements), and also along with either the latest full BAO data set, only Ly-α BAO data, or without BAO data. Then, in the light of the results we have obtained, we extend the discussions on the H_0, M_B, S_8, Ly-α, and ω_b discrepancies made in Ref. [89]; furthermore, we add the t_0 tension to our discussions and give a theoretical explanation of how the S_8 tension is alleviated in Λ_sCDM.

III. OBSERVATIONAL ANALYSIS

Considering the background and perturbation dynamics, in what follows we explore the full parameter space of the Λ_sCDM model and, for comparison, that of the standard ΛCDM model. The baseline seven free parameters of the Λ_sCDM model are given by

$$\mathcal{P} = \{\omega_b, \omega_c, \theta_s, A_s, n_s, \tau_{reio}, z_\dagger\}. \tag{2}$$

Here, the first six parameters are the common ones with the standard ΛCDM model, viz., $\omega_b = \Omega_b h^2$ and $\omega_c = \Omega_c h^2$ (Ω being the present-day density parameter) are, respectively, the present-day physical density parameters of baryons and cold dark matter, θ_s is the ratio of the sound horizon to the angular diameter distance at decoupling, A_s is the initial super-horizon amplitude of curvature perturbations at $k = 0.05$ Mpc^{-1}, n_s is the primordial spectral index, and τ_{reio} is the reionization optical depth. We assume three neutrino species, approximated as two massless states and a single massive neutrino of mass $m_\nu = 0.06$ eV. We use uniform priors $\omega_b \in [0.018, 0.024]$, $\omega_c \in [0.10, 0.14]$, $100\theta_s \in [1.03, 1.05]$, $\ln(10^{10}A_s) \in [3.0, 3.18]$, $n_s \in [0.9, 1.1]$, and $\tau_{reio} \in [0.04, 0.125]$ for the common free parameters of the models, and $z_\dagger \in [1, 3]$ for the additional free parameter characterizing the Λ_sCDM model.

TABLE I. Clustering measurements for each of the BAO samples from Ref. [5].

Parameter	$z_{\rm eff}$	$D_V(z)/r_{\rm d}$	$D_M(z)/r_{\rm d}$	$D_H(z)/r_{\rm d}$
MGS	0.15	4.47 ± 0.17	⋯	⋯
BOSS Galaxy	0.38	⋯	10.23 ± 0.17	25.00 ± 0.76
BOSS Galaxy	0.51	⋯	13.36 ± 0.21	22.33 ± 0.58
eBOSS LRG	0.70	⋯	17.86 ± 0.33	19.33 ± 0.53
eBOSS ELG	0.85	$18.33^{+0.57}_{-0.62}$	⋯	⋯
eBOSS Quasar	1.48	⋯	30.69 ± 0.80	13.26 ± 0.55
Lyα-Lyα	2.33	⋯	37.6 ± 1.9	8.93 ± 0.28
Lyα-Quasar	2.33	⋯	37.3 ± 1.7	9.08 ± 0.34

In order to constrain the models, we use the latest *Planck* CMB data combined with other data sets from independent observations. From the *Planck* 2018 legacy data release [130,131], we use measurements of CMB temperature anisotropy and polarization power spectra, their cross-spectra, and lensing power spectrum, viz., (i) the high-ℓ `Plik` likelihood for TT (in the multipole range $30 \leq \ell \leq 2508$), (ii) TE and EE (in the multipole range $30 \leq \ell \leq 1996$), (iii) the low-ℓTT-only ($2 \leq \ell \leq 29$) likelihood based on the `Commander` component-separation algorithm in pixel space, (iv) the low-ℓEE-only ($2 \leq \ell \leq 29$) `SimAll` likelihood, and (v) the CMB lensing power spectrum measurements reconstructed from the temperature 4-point function. Along with the *Planck* CMB data, we use the high-precision BAO measurements at different redshifts up to $z = 3.5$, viz., the BAO measurements compiled in Table I, from final measurements of clustering using galaxies, quasars, and Lyman-α (Ly-α) forests from the *completed* Sloan Digital Sky Survey (SDSS) lineage of experiments in large-scale structure [5]. It is worth noting that we include the Ly-α measurements in our BAO compilation as these have a substantial impact on the parameters of $\Lambda_{\rm s}$CDM, whereas these have a minor impact on the parameters of ΛCDM, which is why the Ly-α measurements were excluded from the default BAO compilation by the *Planck* (2018) Collaboration [3]. In our analyses, we first consider only the Ly-α data and then the full set of BAO data. We use the Pantheon [132] distance moduli measurements for Type Ia Supernovae which provide the constraints on the slope of the late-time expansion rate $H_0 d_L(z)$, i.e., the noncalibrated light distance. The theoretical apparent magnitude m_B of an SNIa at redshift z reads $m_B(z) = 5\log_{10}[d_L(z)/1\ \text{Mpc}] + 25 + M_B$, where M_B is the absolute magnitude. The distance modulus is then given by $\mu(z) = m_B - M_B$. We constrain the models also by using a Gaussian prior on M_B, viz., $M_B = -19.2435 \pm 0.0373$ mag that corresponds to the SH0ES SNIa measurements [124]—alternatively, one could prefer using an H_0 prior; see Footnote 6 in Sec. IV A for advantages and disadvantages of using M_B or H_0 as a prior. We use the publicly available Boltzmann code CLASS [133] with the parameter inference code MONTE PYTHON [134] to obtain correlated Monte Carlo Markov Chain (MCMC) samples. We analyze the MCMC samples using the python package GetDist; and use the MCEvidence [135] algorithm to approximate the Bayesian evidence, used to perform a model comparison through the Jeffreys' scale [136]. See Ref. [137], and references therein, for an extended review of the cosmological parameter inference and model selection procedure. In general, for a data set D and a given model $\mathcal{M}_a$ with a set of parameters Θ, Bayes' theorem results in

$$P(\Theta|D,\mathcal{M}_a) = \frac{\mathcal{L}(D|\Theta,\mathcal{M}_a)\pi(\Theta|\mathcal{M}_a)}{\mathcal{E}(D|\mathcal{M}_a)}, \tag{3}$$

where $P(\Theta|D,\mathcal{M}_a)$ is the posterior probability distribution function of the parameters, $\pi(\Theta|\mathcal{M}_a)$ is the prior for the parameters, $\mathcal{L}(D|\Theta,\mathcal{M}_a)$ is the likelihood function, and $\mathcal{E}(D|\mathcal{M}_a)$ is the Bayesian evidence given by

$$\mathcal{E}(D|\mathcal{M}_a) = \int_{\mathcal{M}_a} \mathcal{L}(D|\Theta,\mathcal{M}_a)\pi(\Theta|\mathcal{M}_a)\mathrm{d}\Theta. \tag{4}$$

To make a comparison of the model $\mathcal{M}_a$ with some other model $\mathcal{M}_b$, we compute the ratio of the posterior probabilities of the models, given by

$$\frac{P(\mathcal{M}_a|D)}{P(\mathcal{M}_b|D)} = B_{ab}\frac{P(\mathcal{M}_a)}{P(\mathcal{M}_b)}, \tag{5}$$

where B_{ab} is the Bayes' factor given by

$$B_{ab} = \frac{\mathcal{E}(D|\mathcal{M}_a)}{\mathcal{E}(D|\mathcal{M}_b)} \equiv \frac{\mathcal{Z}_a}{\mathcal{Z}_b}. \tag{6}$$

So the relative log-Bayesian evidence reads as

$$\ln B_{ab} = \ln \mathcal{Z}_a - \ln \mathcal{Z}_b \equiv \Delta \ln \mathcal{Z}. \tag{7}$$

The model with smaller $|\ln \mathcal{Z}|$ is the preferred model, and therefore considered as the reference model in model comparison. To interpret the results, we refer to the revised Jeffreys' scale as given in Ref. [138]. Accordingly, a weak evidence is indicated by $0 \leq |\Delta \ln \mathcal{Z}| < 1$, a definite evidence $1 \leq |\Delta \ln \mathcal{Z}| < 3$, a strong evidence by $3 \leq |\Delta \ln \mathcal{Z}| < 5$, and a very strong evidence by $|\Delta \ln \mathcal{Z}| \geq 5$, in favor of the reference model.

In Ref. [89], the authors investigated the observational constraints on the parameters of the models, $\Lambda_{\rm s}$CDM and ΛCDM, with the CMB and CMB + BAO data. In the present study, we obtain the observational constraints on the parameters of these models by using the data combinations of CMB + Pan, CMB + Pan + Ly-α, and CMB + Pan + BAO without and with M_B prior separately present in Tables II and III, respectively. Also, see Figs. 6–11 in Appendix for the corresponding one- and two-dimensional

TABLE II. Constraints (68% CL) on the free and some derived parameters of the Λ_sCDM and standard ΛCDM models for CMB + Pan, CMB + Pan + Ly-α and CMB + Pan + BAO data. In the last three rows, the best fit ($-2\ln\mathcal{L}_{\max}$), the log-Bayesian evidence ($\ln\mathcal{Z}$), and the relative log-Bayesian evidence $\Delta\ln\mathcal{Z}$ [see Eq. (7)] are listed. For each combination of data sets, the model with $\Delta\ln\mathcal{Z}=0$ is the reference (preferred) model.

	CMB + Pan		CMB + Pan + Ly-α		CMB + Pan + BAO	
Data set	ΛCDM	Λ_sCDM	ΛCDM	Λ_sCDM	ΛCDM	Λ_sCDM
$10^2\omega_b$	2.240 ± 0.015	2.241 ± 0.014	2.242 ± 0.013	2.241 ± 0.015	2.242 ± 0.013	2.235 ± 0.014
ω_c	0.1197 ± 0.0012	0.1196 ± 0.0011	0.1193 ± 0.0009	0.1196 ± 0.0011	0.1193 ± 0.0009	0.1206 ± 0.0010
$100\theta_s$	1.04191 ± 0.00029	1.04190 ± 0.00028	1.04191 ± 0.00029	1.04190 ± 0.00029	1.04194 ± 0.00028	1.04180 ± 0.00030
$\ln(10^{10}A_s)$	3.047 ± 0.015	3.041 ± 0.014	3.047 ± 0.014	3.040 ± 0.015	3.047 ± 0.015	3.040 ± 0.014
n_s	0.9662 ± 0.0042	0.9668 ± 0.0040	$0.9669^{+0.0039}_{-0.0036}$	0.9668 ± 0.0041	0.9665 ± 0.0037	0.9644 ± 0.0037
τ_{reio}	0.0556 ± 0.0075	0.0533 ± 0.0075	0.0560 ± 0.0069	0.0528 ± 0.0077	0.0561 ± 0.0076	0.0515 ± 0.0073
$z_\dagger$		>1.80 (95% CL)		$2.21^{+0.16}_{-0.38}$		>2.13 (95% CL)
M_B [mag]	-19.421 ± 0.014	$-19.363^{+0.021}_{-0.037}$	-19.418 ± 0.011	-19.349 ± 0.028	-19.418 ± 0.012	-19.387 ± 0.015
Ω_m	0.3129 ± 0.0071	$0.2940^{+0.0120}_{-0.0093}$	0.3110 ± 0.0053	0.2899 ± 0.0097	0.3109 ± 0.0056	0.3039 ± 0.0058
ω_m	0.1427 ± 0.0011	0.1427 ± 0.0010	0.1424 ± 0.0008	0.1426 ± 0.0010	0.1424 ± 0.0009	0.1436 ± 0.0010
H_0 [km/s/Mpc]	67.55 ± 0.53	$69.68^{+0.77}_{-1.40}$	67.68 ± 0.40	$70.17^{+0.96}_{-1.10}$	$67.69^{+0.38}_{-0.43}$	$68.74^{+0.49}_{-0.55}$
t_0 [Gyr]	13.79 ± 0.02	$13.65^{+0.06}_{-0.04}$	13.79 ± 0.02	$13.62^{+0.09}_{-0.03}$	13.79 ± 0.02	$13.71^{+0.03}_{-0.02}$
σ_8	$0.8111^{+0.0056}_{-0.0063}$	$0.8167^{+0.0059}_{-0.0067}$	0.8104 ± 0.0060	0.8182 ± 0.0066	0.8101 ± 0.0063	0.8167 ± 0.0062
S_8	0.828 ± 0.013	0.809 ± 0.015	0.825 ± 0.010	0.804 ± 0.014	0.825 ± 0.011	0.822 ± 0.010
$-2\ln\mathcal{L}_{\max}$	3807.24	3805.00	3819.36	3806.88	3819.26	3819.06
$\ln\mathcal{Z}$	-1937.82	-1938.02	-1944.53	-1939.75	-1944.51	-1944.76
$\Delta\ln\mathcal{Z}$	0	0.20	4.78	0	0	0.25

TABLE III. Constraints (68% CL) on the free and some derived parameters of the Λ_sCDM and standard ΛCDM models for CMB + Pan, CMB + Pan + Ly-α and CMB + Pan + BAO data with the SH0ES M_B prior. In the last three rows, the best fit ($-2\ln\mathcal{L}_{\max}$), the log-Bayesian evidence ($\ln\mathcal{Z}$), and the relative log-Bayesian evidence $\Delta\ln\mathcal{Z}$ [see Eq. (7)] are listed. For each combination of data sets, the model with $\Delta\ln\mathcal{Z}=0$ is the reference (preferred) model.

	CMB + Pan + M_B		CMB + Pan + Ly-α + M_B		CMB + Pan + BAO + M_B	
Data set	ΛCDM	Λ_sCDM	ΛCDM	Λ_sCDM	ΛCDM	Λ_sCDM
$10^2\omega_b$	2.256 ± 0.015	2.248 ± 0.014	2.253 ± 0.013	$2.247^{+0.014}_{-0.013}$	2.255 ± 0.013	2.242 ± 0.014
ω_c	0.1181 ± 0.0011	0.1191 ± 0.0011	0.1183 ± 0.0008	0.1191 ± 0.0011	0.1181 ± 0.0009	$0.1200^{+0.0010}_{-0.0011}$
$100\theta_s$	1.04208 ± 0.00029	1.04197 ± 0.00031	1.04204 ± 0.00028	1.04196 ± 0.00028	$1.04207^{+0.00029}_{-0.00026}$	1.04186 ± 0.00028
$\ln(10^{10}A_s)$	$3.053^{+0.014}_{-0.017}$	3.039 ± 0.014	$3.052^{+0.013}_{-0.016}$	3.041 ± 0.015	$3.053^{+0.014}_{-0.016}$	3.041 ± 0.015
n_s	0.9701 ± 0.0040	$0.9687^{+0.0043}_{-0.0038}$	0.9697 ± 0.0035	0.9684 ± 0.0041	0.9702 ± 0.0035	0.9661 ± 0.0037
τ_{reio}	$0.0601^{+0.0072}_{-0.0085}$	0.0526 ± 0.0074	$0.0593^{+0.0064}_{-0.0079}$	0.0535 ± 0.0077	$0.0603^{+0.0070}_{-0.0078}$	0.0524 ± 0.0076
$z_\dagger$		$1.78^{+0.14}_{-0.18}$		$1.84^{+0.13}_{-0.21}$		2.36 ± 0.28
M_B [mag]	-19.399 ± 0.014	$-19.290^{+0.026}_{-0.029}$	-19.402 ± 0.011	-19.299 ± 0.028	-19.399 ± 0.011	$-19.366^{+0.013}_{-0.015}$
Ω_m	0.3028 ± 0.0068	0.2716 ± 0.0084	0.3043 ± 0.0050	$0.2743^{+0.0086}_{-0.0097}$	0.3030 ± 0.0051	0.2965 ± 0.0055
ω_m	0.1413 ± 0.0011	0.1422 ± 0.0010	0.1415 ± 0.0008	0.1422 ± 0.0011	0.1413 ± 0.0008	0.1431 ± 0.0010
H_0 [km/s/Mpc]	68.31 ± 0.52	$72.38^{+0.98}_{-1.10}$	68.19 ± 0.38	72.0 ± 1.1	68.29 ± 0.39	$69.48^{+0.48}_{-0.55}$
t_0 [Gyr]	13.76 ± 0.02	13.55 ± 0.05	13.76 ± 0.02	$13.56^{+0.04}_{-0.04}$	13.76 ± 0.02	13.67 ± 0.03
σ_8	0.8090 ± 0.0064	$0.8255^{+0.0072}_{-0.0081}$	$0.8091^{+0.0054}_{-0.0063}$	0.8243 ± 0.0076	$0.8092^{+0.0057}_{-0.0061}$	0.8176 ± 0.0063
S_8	0.813 ± 0.012	0.785 ± 0.012	0.815 ± 0.010	$0.788^{+0.012}_{-0.014}$	0.813 ± 0.010	0.813 ± 0.010
$-2\ln\mathcal{L}_{\max}$	3826.56	3808.58	3837.36	3811.76	3839.70	3831.14
$\ln\mathcal{Z}$	-1947.83	-1940.06	-1954.17	-1941.85	-1955.02	-1951.79
$\Delta\ln\mathcal{Z}$	7.77	0	12.32	0	3.23	0

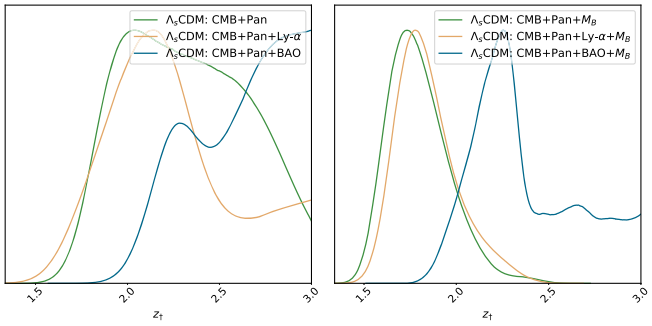

FIG. 1. One-dimensional marginalized posterior distributions of the parameter $z_\dagger$ of the Λ_sCDM model, the redshift at which the cosmological constant (Λ_s) changes sign, for various data set combinations.

[at 68% and 95% confidence levels (CLs)] marginalized distributions of the model parameters.[5] In the last three rows of these tables, we list the best fit ($-2\ln\mathcal{L}_{\max}$), the log-Bayesian evidence ($\ln\mathcal{Z}$), and the log-Bayesian evidence relative to the reference model ($\Delta\ln\mathcal{Z}$).

The distinctive free parameter of the Λ_sCDM model is $z_\dagger$, the redshift at which the cosmological constant (Λ_s) changes sign. In Fig. 1, we present the one-dimensional marginalized distributions of the parameter $z_\dagger$ for various data set combinations. From Ref. [89], we know that the CMB data alone is not able to constrain $z_\dagger$, implying that any $z_\dagger \gtrsim 1.5$ (1.5 is the lower limit of the prior used in Ref. [89]), i.e., a negative cosmological constant $\Lambda_s(z > z_\dagger) = -\Lambda_{s0} \sim -2.9 \times 10^{-122} l_{\rm Planck}^{-2}$ is consistent with the CMB data. But when the SNIa data are included in the analysis with CMB (see the green curve in Fig. 1), the shape of the distribution changes, and we find lower bound of $z_\dagger > 1.77$ and with the inclusion of the Ly-α data (which favor $z_\dagger$ values less than ∼2.33) as well, we see a clear peak at $z_\dagger \sim 2.2$ with a plateaulike tail for $z_\dagger \gtrsim 2.5$, the region where the model approaches ΛCDM. However, with the inclusion of the full BAO data, rather than only the Ly-α data, again we find only a lower bound, $z_\dagger > 2.13$. This is because the low-redshift BAO data tend to push $z_\dagger$ to larger values, despite the opposition of the Ly-α; this point was discussed in Ref. [89] thoroughly, also see Sec. IV D. We notice that including the M_B prior in the analysis has important consequences in the results. When the M_B prior is present, whether the Ly-α data are included or not on top of CMB + Pan data, $z_\dagger$ is very well constrained at $z \approx 1.8$ with ∼10% precision at %68 CL. While the CMB + Pan + BAO data combination without the M_B prior is able to provide only a lower bound on $z_\dagger$, with the M_B prior it leads to a clear peak at $z \approx 2.3$ with ∼10% precision at %68 CL, with a flat tail for $z \gtrsim 2.4$ seems to have arisen from the preference of higher $z_\dagger$ values of the low-redshift BAO data.

In Ref. [89], no strong statistical evidence was found to discriminate between the Λ_sCDM and ΛCDM models in the analyses with neither the CMB data nor the CMB + BAO data (estimates $z_\dagger \sim 2.4$). We see in the current work that, without the M_B prior, this picture does not change for the cases CMB + Pan (estimates $z_\dagger \gtrsim 1.8$) and CMB + Pan + BAO (estimates $z_\dagger \gtrsim 2.1$), while the Λ_sCDM model finds a strong evidence ($\Delta\ln\mathcal{Z} \sim 5$) against the standard ΛCDM model for the case CMB + Pan + Ly-α (estimates $z_\dagger \sim 2.2$); see Table II. On the other hand, when we analyze the models with the same data sets by including the M_B prior that corresponds to the SH0ES SNIa measurements [124], it turns out that the Λ_sCDM model (estimates $z_\dagger \sim 2$) is always preferred over the standard ΛCDM model; namely, Λ_sCDM finds very strong evidence (reaching $\Delta\ln\mathcal{Z} \sim 12$) against ΛCDM by predicting $z_\dagger \sim 1.8$ for both the CMB + Pan + M_B and CMB + Pan + Ly-α + M_B cases, and finds strong evidence ($\Delta\ln\mathcal{Z} \sim 3$) by predicting $z_\dagger \sim 2.4$ for the CMB + Pan + BAO + M_B case; see Table III. Hence, the relative log-Bayesian evidences are significantly strengthened in favor of Λ_sCDM in all cases with the inclusion of M_B prior. Regarding the best fits ($-2\ln\mathcal{L}_{\max}$), the inclusion of the M_B prior results in a substantial worsening ($-2\Delta\ln\mathcal{L}_{\max} \sim 20$) of ΛCDM's fit to the data for all three data compilations; compare $-2\ln\mathcal{L}_{\max}$ of Tables II and III. On the other hand, for Λ_sCDM, there is no significant worsening ($-2\Delta\ln\mathcal{L}_{\max} \sim 5$) without the full BAO data, and while it becomes noticeable ($-2\Delta\ln\mathcal{L}_{\max} \sim 12$) when the full BAO data is included, it still is milder compared to ΛCDM. This implies that Λ_sCDM has much better consistency with the M_B prior than ΛCDM and signals Λ_sCDM relaxes the M_B tension and thus the closely related H_0 tension as well. Also, in both tables (Tables II and III), we see that the expansion of CMB + Pan and CMB + Pan + M_B analyzes by including the Ly-α data makes a significant improvement (∼5) in the relative log-Bayesian evidence in favor of Λ_sCDM, which indicates that Λ_sCDM is also highly compatible with the Ly-α data. On the other hand, when we expand the CMB + Pan and CMB + Pan + M_B analyzes by including the full BAO data listed in Table I (equivalent to expanding the cases CMB + Pan + Ly-α and CMB + Pan + Ly-α + M_B by adding the low-redshift BAO data) we compromise on this improvement; namely, the strong evidence ($\Delta\ln\mathcal{Z} \sim 5$) from the CMB + Pan + Ly-α data set in favor of Λ_sCDM is lost ($\Delta\ln\mathcal{Z} \sim 0$) in the CMB + Pan + BAO case, and the very strong evidence ($\Delta\ln\mathcal{Z} \sim 12$) from the CMB + Pan + Ly-α + M_B data set in favor of Λ_sCDM is reduced to strong evidence ($\Delta\ln\mathcal{Z} \sim 3$) in the CMB + Pan + BAO + M_B case. It is worth mentioning here that the Ly-α data support $z_\dagger$ values less than ∼2.3, whereas some low-redshift BAO data prefer $z_\dagger$ values

[5]Note that the BAO data used in the present study is an updated and extended version of that in Ref. [89], hence the results are not directly comparable.

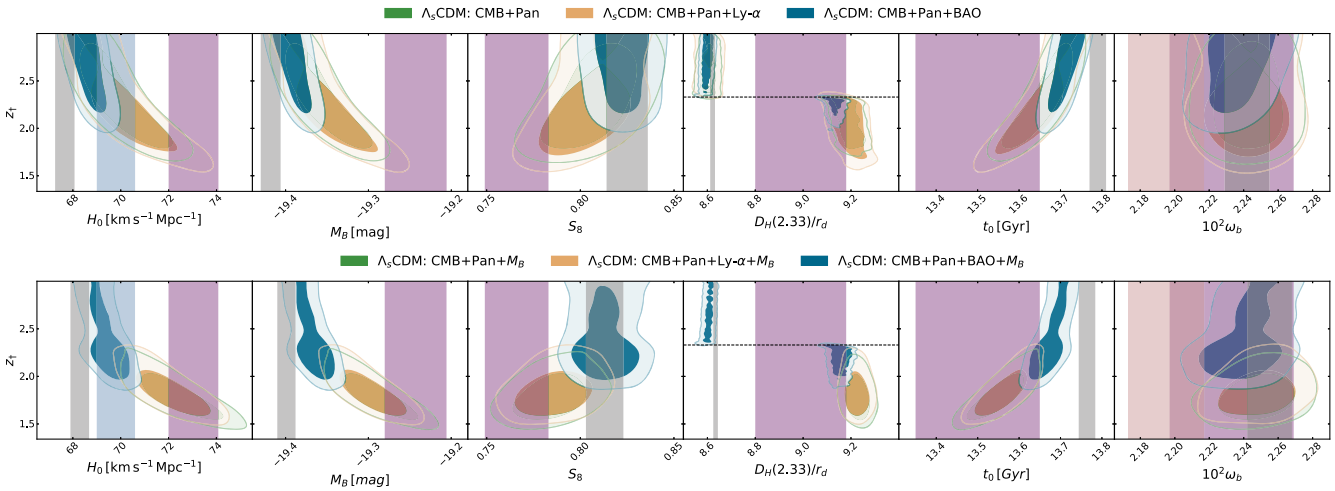

FIG. 2. Two-dimensional marginalized probability posteriors of $z_\dagger$ versus H_0, M_B, S_8, $D_H(2.33)/r_\mathrm{d}$ (D_H/r_d at $z_\mathrm{eff}=2.33$ relevant to the Ly-α measurements), t_0, and ω_b in Λ_sCDM model from various combinations of the data sets. The vertical gray bands are the constraints (68% CL) for the ΛCDM model, where in the upper panels we consider only CMB + Pan + BAO and in the lower panels CMB + Pan + BAO + M_B since the vertical gray bands obtained for other combinations of data sets do not differ visually. The vertical purple bands stand for the theoretical/direct observational estimations (at 68% CL) of the corresponding parameters commonly used in the literature: $H_0^{\mathrm{R21}}=73.04\pm1.04$ km s^{-1} Mpc^{-1} [18]; $M_B=-19.244\pm0.037$ mag (SH0ES) [124]; $S_8=0.766^{+0.020}_{-0.014}$ (WL + GC KiDS-1000 3×2pt) [139]; $D_H(2.33)/r_\mathrm{d}=8.99\pm0.19$ (for combined Ly-α data) [140]; $t_\mathrm{u}=13.50\pm0.15$ Gyr (systematic uncertainties are not included) [141]; $10^2\omega_\mathrm{b}^{\mathrm{LUNA}}=2.233\pm0.036$ [128]. In addition, we show vertical blue and brown bands for $H_0^{\mathrm{TRGB}}=69.8\pm0.8$ km s^{-1} Mpc^{-1} [118] and $10^2\omega_\mathrm{b}^{\mathrm{PCUV21}}=2.195\pm0.022$ [142], respectively. Note that the disjoint contours (around the horizontal $z_\dagger=2.33$ dashed line) of Λ_sCDM for $D_H(2.33)/r_\mathrm{d}$ are as expected since Λ_s at $z=2.33$ is negative for $z_\dagger<2.33$ and positive for $z_\dagger>2.33$.

greater than ∼2.3, forcing the Λ_sCDM model to its ΛCDM limit ($z_\dagger\to\infty$).

IV. RELAXING COSMOLOGICAL TENSIONS

As we discussed in the previous section, the Λ_sCDM model generically finds better fit to the data compared to the ΛCDM model. Since the inclusion of the M_B prior and/or the Ly-α data in the data sets causes Λ_sCDM to perform even better compared to ΛCDM, we expect it to resolve, or at least relax, the M_B and the closely related H_0 tensions along with the Ly-α discrepancy. In Fig. 2, we show the two-dimensional marginalized probability posteriors of $z_\dagger$ versus H_0, M_B, S_8, $D_H(2.33)/r_\mathrm{d}$ (viz., the D_H/r_d at $z_\mathrm{eff}=2.33$ relevant to the Ly-α measurements), t_0, and ω_b in the Λ_sCDM model from various combinations of the data sets and in Table IV we quantify the concordances/discordances between the ΛCDM and Λ_sCDM models and the theoretical/direct observational estimations, viz., $H_0^{\mathrm{R21}}=73.04\pm1.04$ km s^{-1} Mpc^{-1} [18] and $H_0^{\mathrm{TRGB}}=69.8\pm0.8$ km s^{-1} Mpc^{-1} [118]; $M_B=-19.244\pm0.037$ mag (SH0ES) [124]; $S_8=0.766^{+0.020}_{-0.014}$ (WL + GC KiDS-1000 3×2pt) [139]; $D_H(2.33)/r_\mathrm{d}=8.99\pm0.19$ (for the combined Ly-α data) [140]; $t_0=13.50\pm0.27$ Gyr [141]; $10^2\omega_\mathrm{b}^{\mathrm{LUNA}}=2.233\pm0.036$ [128] and $10^2\omega_\mathrm{b}^{\mathrm{PCUV21}}=2.195\pm0.022$ [142]. In what follows, we discuss these tensions and how they are relaxed within the Λ_sCDM model compared to the ΛCDM model.

A. H_0 discrepancy

The most statistically significant and pressing tension is in H_0, between its direct local distance ladder measurements and its estimations from the CMB data assuming the standard ΛCDM model. More precisely, there exists approximately 5σ tension between its ΛCDM value $H_0=67.27\pm0.60$ km s^{-1} Mpc^{-1} (68% CL) [3] inferred from *Planck* 2018 and the SH0ES measurement $H_0=73.04\pm1.04$ km s^{-1} Mpc^{-1} (68% CL) [18] based on the SNIa calibrated by Cepheid variables. This tension reduces to a mild discrepancy of 2.5σ (or 2.7σ) when the TRGB measurement $H_0=69.8\pm0.8$ km s^{-1} Mpc^{-1} (68% CL) [118] (or $H_0=69.8\pm0.6$ km s^{-1} Mpc^{-1} [126], at 68% CL), which is 2.5σ (or 2.7σ) tension with the SH0ES measurement, is considered. There are in fact plenty of other independent (at least partially) and direct H_0 measurements relying on different methods and astrophysical observations [143–151] (see Ref. [15] for a further list of direct H_0 measurements). Almost all of these are statistically consistent with the latest SH0ES measurement, but their error percentages are large compared to those of SH0ES and TRGB measurements. Among these alternatives, the time-delay related measurements (based on

TABLE IV. Concordance/discordance between the ΛCDM/Λ_sCDM models and the theoretical/direct observational estimations, viz., $H_0^{\rm R21} = 73.04 \pm 1.04$ km s^{-1} Mpc^{-1} [18] and $H_0^{\rm TRGB} = 69.8 \pm 0.8$ km s^{-1} Mpc^{-1} [118]; $M_B = -19.244 \pm 0.037$ mag (SH0ES) [124]; $S_8 = 0.766^{+0.020}_{-0.014}$ (WL + GC KiDS-1000 3 × 2pt) [139]; $D_H(2.33)/r_{\rm d} = 8.99 \pm 0.19$ (for the combined Ly-α data) [140]; $t_0 = 13.50 \pm 0.15$ Gyr (systematic uncertainties are not included) [141]; $10^2\omega_{\rm b}^{\rm LUNA} = 2.233 \pm 0.036$ [128] and $10^2\omega_{\rm b}^{\rm PCUV21} = 2.195 \pm 0.022$ [142]. The results marked with * should be interpreted with caution since the SH0ES M_B prior is not fully consistent with the TRGB measurements.

	CMB + Pan		CMB + Pan + Ly-α		CMB + Pan + BAO		CMB + Pan + M_B		CMB + Pan + Ly-α + M_B		CMB + Pan + BAO + M_B	
Data set	ΛCDM	Λ_sCDM	ΛCDM	Λ_sCDM	ΛCDM	Λ_sCDM	ΛCDM	Λ_sCDM	ΛCDM	Λ_sCDM	ΛCDM	Λ_sCDM
$H_0^{\rm R21}$	4.7σ	2.2σ	4.8σ	2.0σ	4.8σ	3.7σ	4.1σ	0.4σ	4.4σ	0.7σ	4.3σ	3.1σ
$H_0^{\rm TRGB}$	2.3σ	0.1σ	2.8σ	0.3σ	2.4σ	1.1σ	1.6σ*	2.0σ*	1.8σ*	1.6σ*	1.7σ*	0.3σ*
M_B	4.5σ	2.5σ	4.5σ	2.3σ	4.5σ	3.6σ	3.9σ	1.0σ	4.1σ	1.2σ	4.0σ	3.1σ
S_8	2.9σ	1.9σ	3.0σ	1.7σ	2.9σ	2.8σ	2.3σ	0.9σ	2.5σ	1.0σ	2.4σ	2.4σ
$D_H(2.33)/r_{\rm d}$	2.0σ	0.2σ	1.9σ	0.1σ	1.9σ	1.1σ	1.9σ	1.2σ	1.8σ	1.2σ	1.9σ	0.1σ
$t_{\rm u}$	1.9σ	1.0σ	1.9σ	0.8σ	1.9σ	1.4σ	1.7σ	0.3σ	1.7σ	0.4σ	1.7σ	1.1σ
$\omega_{\rm b}^{\rm PCUV21}$	1.7σ	1.8σ	1.8σ	1.7σ	1.8σ	1.5σ	2.3σ	2.0σ	2.3σ	2.0σ	2.3σ	1.8σ
$\omega_{\rm b}^{\rm LUNA}$	0.2σ	0.2σ	0.2σ	0.2σ	0.2σ	0.1σ	0.6σ	0.4σ	0.5σ	0.4σ	0.6σ	0.2σ

Ref. [152]) stand out as they are independent of the distance ladders on which SH0ES and TRGB H_0 measurements rely, and as they can provide error percentages comparable to those of SH0ES and TRGB H_0 measurements; namely, $H_0 = 73.3^{+1.7}_{-1.8}$ of H0LiCOW [153] and $H_0 = 74.2 \pm 1.6$ of TDCOSMO [154]—though, their low error percentages require assumptions on the mass density profiles of the deflector galaxies to break the so-called mass-sheet degeneracy, leaving the method prone to systematics; relaxed assumptions on the mass density profile result in looser constraints, e.g., the TDCOSMO results $H_0 = 73.3 \pm 5.8$ [155], and the recent $H_0 = 77.1^{+7.3}_{-7.1}$ [156] from the analysis of a single system.[6]

Consistency with CMB requires that the presence of a sign-switching cosmological constant instead of a regular one always results in a higher H_0 value inversely correlated with $z_\dagger$; this behavior is visible in the leftmost panels of Fig. 2 (for a detailed explanation, see Ref. [89] and particularly Figs. 2 and 8 therein). Hence, the higher H_0 values of Λ_sCDM compared to ΛCDM in Tables II and III for all six data sets are no surprise; and, as seen from Table IV, for all six data sets, Λ_sCDM is in better agreement with the SH0ES H_0 measurement (so also with the H0LiCOW and TDCOSMO H_0 measurements) and is compatible (i.e., discrepancy is less than 2σ) with the TRGB H_0 measurement having at most a 2σ discrepancy in the case of CMB + Pan + M_B and only because it predicts too high of an H_0 value compared to TRGB. Also, note that, the M_B prior we use is that of SH0ES and this must be kept in mind when the constraints on H_0 in its presence are compared with the TRGB H_0 measurement. As seen from Fig. 1, the M_B prior clearly prefers a sign switch at lower

[6]Note that, since some of these H_0 measurements based on the alternative methods are independent of the calibration of supernova absolute magnitudes, deciding to use an H_0 prior instead of an M_B prior allows the usage of a wider variety of measurements related to the present-day expansion of the Universe. We use the SH0ES measurement due to its robustness and reliability, and we chose their M_B estimation as our prior instead of H_0 since M_B is the more direct estimation whereas their inference of H_0 require some minimal assumptions related to low-redshift cosmography (See Sec. IV B). It is possible that a cosmological model agrees with one of these quantities (H_0, M_B) without agreeing with both [157–166]. Thus, if one decides to use an H_0 prior from a certain measurement, they should also compare their results against independent M_B measurements—if the used H_0 prior is inferred from an M_B value, a comparison with that value is also required. Similarly, if one decides to use an M_B prior from a certain measurement, they should also compare their results against independent H_0 measurements—but not necessarily against the H_0 value inferred from that M_B prior. Since almost all direct measurements of H_0 independent of the SH0ES measurement are statistically consistent with the SH0ES value, instead of discussing other independent measurements, we compare our results again with the SH0ES H_0 estimation. Also, due to the discrepancy between the SH0ES and TRGB measurements (note, however, the recent work Ref. [167]), we include comparisons of our results with the TRGB H_0 measurement.

redshifts $1.6 \lesssim z_\dagger \lesssim 2$; thus, when the M_B prior is included in the data sets, the estimations of H_0 within Λ_sCDM are higher compared to the same data sets without the M_B prior due to the inverse correlation of $z_\dagger$ and H_0. This results in removal of the SH0ES H_0 tension for the CMB + Pan + M_B and CMB + Pan + Ly-α + M_B cases. In fact, for these cases, H_0 predictions of Λ_sCDM are high enough that they start introducing mild discrepancies with the TRGB H_0 measurement. In contrast, addition of the M_B prior makes little to no difference for the ΛCDM model in amelioration of the SH0ES H_0 tension.

However, for the CMB + Pan + BAO cases with or without the M_B prior, the preference of high $z_\dagger$ values by the lower redshift BAO hinders the success of Λ_sCDM in ameliorating the discrepancies displayed in Table IV including the SH0ES H_0 tension—the opposition of the low-redshift BAO data (viz., consensus Galaxy BAO from $z_{\rm eff} = 0.38,\ 0.51,\ 0.61$) to lower $z_\dagger$ values and hence to higher H_0 values was discussed in Ref. [89]. Closely related to this, the H_0 tension within ΛCDM not only exists between the local H_0 measurements and the inference of H_0 from CMB, but also between the local H_0 measurements and the BAO data set (combined with a BBN prior) when CMB data set is not used [5,52,168–170]. It is worth mentioning that this tension with the BAO does not originate from any particular BAO measurement, rather, it is due to the different degeneracy directions of the constraints from BAO at redshifts ($z > 1$) and galaxy BAO at low redshifts ($z < 1$) in the $\Omega_m - H_0$ plane; see Refs. [5,52,168–170], for instance, Fig. 5 of Ref. [5]. Here, $\Omega_m \equiv 8\pi G\rho_{m0}/(3H_0^2)$ is the present-day ($z = 0$) matter density parameter with ρ_{m0} being the present-day matter energy density. Note that the CMB agrees very well with the BBN constraints used in Refs. [5,52] and the degeneracy direction of the constraints from high redshift BAO data agrees with that of the CMB within both ΛCDM and Λ_sCDM with contours for Λ_sCDM being shifted to higher H_0 values as indicated by the analyses in Ref. [89]. While Λ_sCDM is able to address the H_0 tension with the CMB, the different degeneracy direction of the galaxy BAO will still introduce problems. That is because, since $z_\dagger > 1$ is satisfied for any reasonable expansion history within Λ_sCDM (see Fig. 5 and the relevant discussion in Ref. [89]), both models are equivalent for the whole range of the galaxy BAO and would yield the same contours in a BBN + galaxy BAO analysis as in Refs. [5,52] and the shift to higher H_0 values within Λ_sCDM in the $\Omega_m - H_0$ plane by itself is not adequate for a full resolution of the BAO-based H_0 tension but only an amelioration. This inadequacy manifests itself in the impairing of Λ_sCDM in alleviating the H_0 tension when the full BAO data is included in our analyses as can be seen from, in addition to Table IV, the blue contours in the H_0 panels of Fig. 2, and particularly clearly by comparing the rightmost panels of Figs. 3 and 4 showing the analyses including the full BAO data to the rest of their panels showing the cases without the low-redshift BAO data.

Another point of interest is the relation of the H_0 tension with the M_B and S_8 tensions (the two other prominent

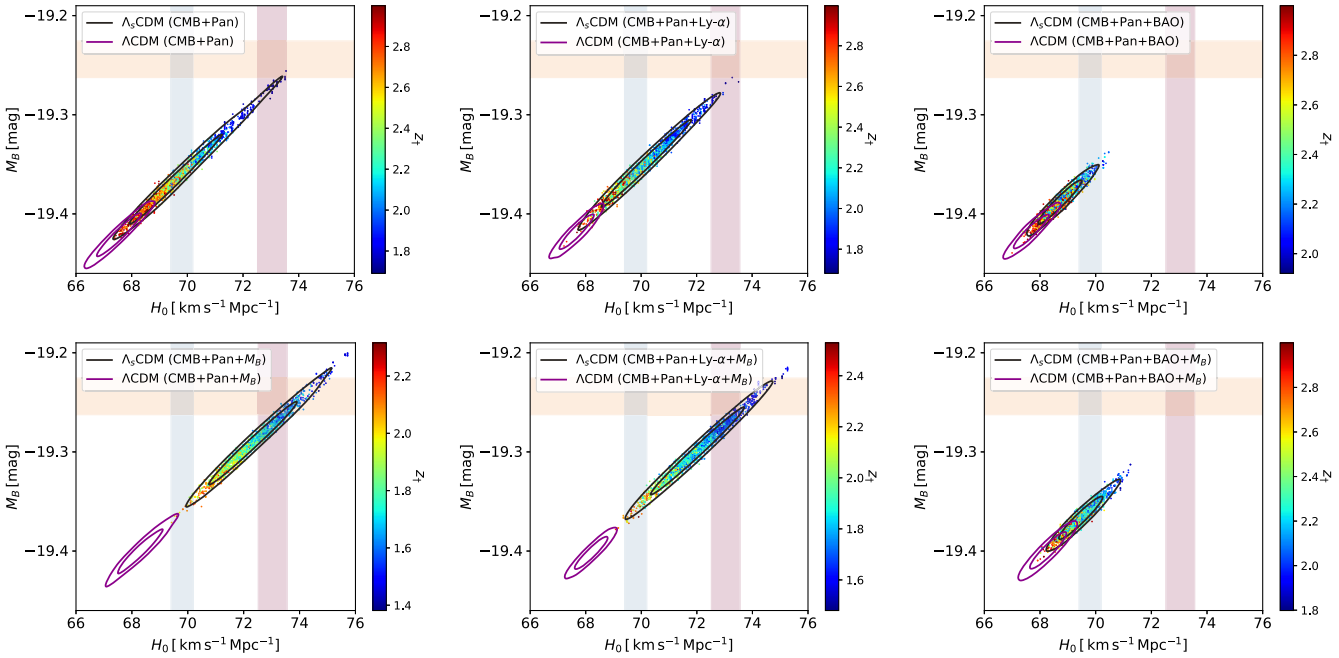

FIG. 3. Two-dimensional marginalized posterior distributions (68% and 95% CLs) in the M_B-H_0 plane for the Λ_sCDM (color coded by $z_\dagger$) and ΛCDM for different data combinations. We overlay 1σ bands for the local measurements $H_0^{R21} = 73.04 \pm 1.04$ km s^{-1} Mpc^{-1} [18], $H_0^{TRGB} = 69.8 \pm 0.8$ km s^{-1} Mpc^{-1} [118], and $M_B = -19.244 \pm 0.037$ mag (SH0ES) [124]. The larger $z_\dagger$ is, the closer the Λ_sCDM model is to the standard ΛCDM model.

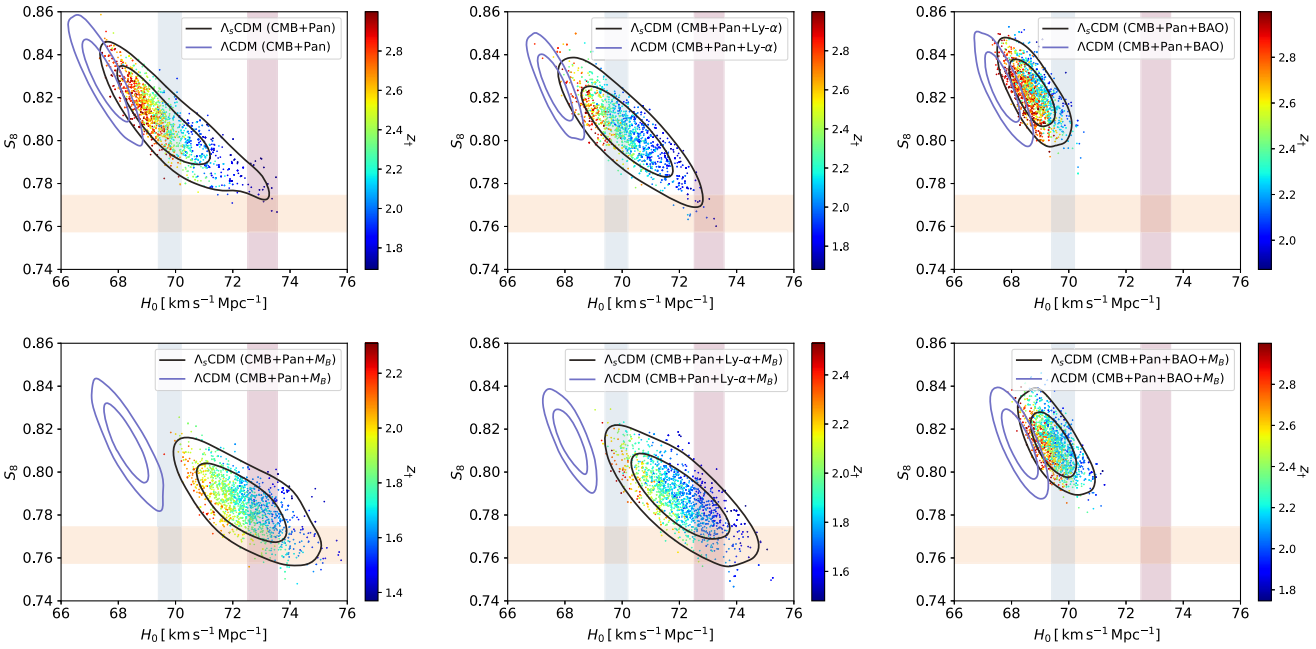

FIG. 4. Two-dimensional marginalized posterior distributions (68% and 95% CLs) in the S_8-H_0 plane for the Λ_sCDM (color coded by $z_\dagger$) and ΛCDM for different data combinations. We overlay 1σ bands for the local measurements $H_0^{\rm R21} = 73.04 \pm 1.04$ km s^{-1} Mpc^{-1} [18], $H_0^{\rm TRGB} = 69.8 \pm 0.8$ km s^{-1} Mpc^{-1} [118], and $S_8 = 0.766^{+0.020}_{-0.014}$ (WL + GC KiDS-1000 3 × 2pt) [139]. The larger $z_\dagger$ is, the closer the Λ_sCDM model is to the standard ΛCDM model.

discrepancies of ΛCDM) within Λ_sCDM. The two-dimensional marginalized posterior distributions of M_B versus H_0, and S_8 versus H_0 are given in Figs 3 and 4, respectively, both color coded by $z_\dagger$. These two figures have some striking common features: (i) there is a strong correlation with H_0 and the other two parameters; (ii) lower $z_\dagger$ values are preferred by all three discrepancies; (iii) the presence of the full BAO data set hinders the alleviation of the tensions by preferring higher $z_\dagger$ values that blur the phenomenological differences between the two models; and (iv) the presence of the M_B prior results in better alleviation of the tensions and greater differentiation between the two models by preferring lower $z_\dagger$ values. The correlation is particularly pronounced between M_B and H_0; the analyses without the full BAO data yield a correlation of ∼0.99 and the ones with the full BAO data yield ∼0.96.

B. M_B discrepancy

The M_B tension is closely related to the H_0 tension [15,124,171] (see also Refs. [157–159]). The local H_0 measurements rely on observations of astrophysical objects that extend into redshifts where the Hubble flow dominates over peculiar velocities. Particularly, the two most quoted measurements of H_0, namely the TRGB and SH0ES values, are based on the calibration (using Cepheid variables for SH0ES, and tip of the red giant branch for TRGB) of the SNIa absolute magnitude. From the calibrated absolute magnitude, using the apparent magnitudes of SNIa that extend up to $z = 0.15$, the value of H_0 is then inferred by assuming a ΛCDM-like cosmography for which the distance modulus $\mu(z)$ depends only on H_0. This H_0 value, as discussed in the previous subsection, is in substantial tension with the one inferred from the CMB assuming ΛCDM cosmology. This implies a serious inconsistency between the CMB and local measurements. This inconsistency is also present if, instead of propagating the local calibration of M_B to an H_0 value, one propagates the constraints on $r_{\rm d}$ from CMB to constraints on M_B through the inverse distance ladder as in Ref. [171] utilizing BAO measurements. The CMB calibration yields $M_B^{\rm CMB} = -19.401 \pm 0.027$ mag [171] while the SH0ES calibration yields $M_B = -19.2435 \pm 0.0373$ mag [124]. Alternatively, instead of comparing the local H_0 value (inferred from the Cepheid or TRGB calibrated M_B value) with the H_0 value inferred by constraining the parameters of a model (most often making use of the CMB), one can calculate the distance modulus for the constrained model which can be used to infer the SNIa absolute magnitude (M_B) from their apparent magnitudes, and then directly compare this M_B value with the one calibrated using Cepheid variables or TRGB. Within ΛCDM, where the cosmographic assumptions used in the inference of the local H_0 measurements are accurate, the M_B and H_0 tensions are almost equivalent. It is important to note that, for an arbitrary model, the direct comparison of the M_B values instead of H_0 is advantageous as this method is not

prone to finding fake resolutions of the H_0 tension as discussed in Refs. [160–166].

Since the SH0ES H_0 measurement is based on a ΛCDM-like cosmography to infer H_0 from the M_B value found by the calibration of SNIa up to $z = 0.15$ by Cepheid variables from $z < 0.01$, within Λ_sCDM, for which the functional form of the cosmographic parameters are exactly those of ΛCDM for $z < z_\dagger$, the resolution of the H_0 and M_B tensions are almost equivalent just as it is within ΛCDM (note that the constraint on $z_\dagger$ is well above the redshift range of the SNIa data used by the local measurements [18,118], and is greater than most of the available SNIa sample [132]). In other words, the Λ_sCDM model respects the internal consistency of the methodology used by the SH0ES collaboration. Figure 3 and the almost perfect correlation between H_0 and M_B within Λ_sCDM (see the end of Sec. IV A) clearly illustrate this feature; also compare the first and third rows of Table IV. As a result, the discussion for the M_B tension follows the H_0 tension discussion in the previous subsection very closely. For all six data sets, Λ_sCDM yields higher (fainter) M_B values compared to ΛCDM as shown in Tables II and III. Higher M_B values are also what the local calibrations find, and this is reflected in Table IV where, compared to ΛCDM, Λ_sCDM is always in less tension. As in the case of the H_0 tension, the inclusion of the M_B prior reduces the M_B tension significantly for Λ_sCDM for all three data compilations (down to 1σ for the CMB + Pan + M_B case) and the inclusion of the full BAO in the compilation has a hindering effect. Note that, in contrast, the addition of the M_B prior makes little to no difference for the ΛCDM model in amelioration of the M_B tension.

C. S_8 discrepancy

There is a discordance within ΛCDM between CMB and dynamical low-redshift cosmological probes (weak lensing, cluster counts, redshift-space distortion) that manifests itself in the $\sigma_8 - \Omega_m$ plane, where the σ_8 parameter quantifying the amplitude of growth of structure is the root-mean-square of the present-day matter density fluctuations within spheres of $8h^{-1}$ Mpc. This discordance is typically quantified by the $S_8 \equiv \sigma_8\sqrt{\Omega_m/0.3}$ parameter that characterizes the main degeneracy direction of the weak lensing measurements in the $\sigma_8 - \Omega_m$ plane. Assuming the ΛCDM model, the CMB constraints on S_8 from the full Planck data yield $S_8 = 0.834 \pm 0.016$ [3] up to 3σ tension with the low-redshift measurements such as $S_8 = 0.766^{+0.020}_{-0.014}$ (WL + GC KiDS-1000 3×2pt) [139], and $S_8 = 0.759 \pm 0.025$ (DES-Y3) [172]—although, note the Hyper Suprime-Cam (HSC) measurement $S_8 = 0.823^{+0.032}_{-0.028}$ [173] that is consistent with the Planck ΛCDM value. Thus, the resolution of this discrepancy within a different model calls for a reduced S_8 prediction without compromising the agreement with the CMB. While this implies a reduction in the values of the parameters σ_8 and Ω_m, it is possible that a significant enough reduction in the value of either of the parameters can work just as well even if the remaining one's value is increased. Indeed, the observational assessments of ΛCDM and Λ_sCDM in Ref. [89] presented higher σ_8 values for the Λ_sCDM model, and the CMB-only data set yielded a matter density parameter value of $\Omega_m = 0.2900 \pm 0.0160$ for Λ_sCDM lower compared to the ΛCDM value of $\Omega_m = 0.3162 \pm 0.0084$, overcompensating the Λ_sCDM's increased σ_8 parameter and consequently resulting in a relaxed $S_8 = 0.8071 \pm 0.0210$ value compared to the $S_8 = 0.8332 \pm 0.0163$ of ΛCDM. Pleasantly, this amelioration of the S_8 tension is closely related to the amelioration of the H_0 tension within the Λ_sCDM model as its reduced Ω_m value is not due to a reduced physical matter density but its increased H_0 value. Note that, relaxing the S_8 tension is not a generic property of models that relax the H_0 tension, on the contrary, they often exacerbate it due to an excessively large σ_8 parameter [11,15]. For instance, amongst many, EDE [19–22], as well as related models such as new-EDE [23,24], is one of the most popular promising ones for relaxing the H_0 tension, however both EDE and new-EDE exacerbate the S_8 tension. AdS-EDE [69,75,102] is especially worth mentioning, because, similar to Λ_sCDM, it is based on an AdS-dS transition. On the other hand, Λ_sCDM considers the possibility of a rapid AdS-dS transition at redshift $z \sim 2$, whereas AdS-EDE has an AdS phase that begins at $z \sim 2000$ and ends shortly after recombination ($z_{rec} \simeq 1100$), settling down in a $\Lambda > 0$ (dS) phase that still continues today. However, AdS-EDE, like other EDE models, relaxes the H_0 tension but worsens the S_8 tension [102].

To understand the structure formation within Λ_sCDM and how it compares to ΛCDM, we start with the Newtonian equation for the growth of structure of the minimally interacting pressureless sources (baryons and CDM) after decoupling,

$$\partial_t^2\delta_m = -2H\partial_t\delta_m + 4\pi G\bar{\rho}_m\delta_m, \tag{8}$$

where $\bar{\rho}_m$ is the spatially uniform background energy density and δ_m is the fractional overdensity of the pressureless fluid [174]. We take $\delta_m = \frac{\bar{\rho}_b\delta_b + \bar{\rho}_c\delta_c}{\bar{\rho}_b + \bar{\rho}_c} \approx \delta_b \approx \delta_c$ as quickly after recombination, the fractional overdensity in the baryons, δ_b, approaches that of the CDM, δ_c, and the matter behaves like a single pressureless fluid with total density contrast δ_m. The first term in the right-hand side, yielding negative values (assuming expanding universe, $H > 0$), is antagonist to the growth of structure, and the second term, yielding positive values, endorses the growth of structure. We recall that the Hubble parameters, assuming expanding universe, are given by $H_{\Lambda CDM} = \sqrt{8\pi G\bar{\rho}_m/3 + \Lambda/3}$ for ΛCDM, and $H_{\Lambda_s CDM} = \sqrt{8\pi G\bar{\rho}_m/3 + \Lambda_s/3}$ for Λ_sCDM, where we work in units

such that the speed of light, c, equals unity. Thus, if both models have the same initial conditions for $\bar{\rho}_{\rm m}$ before the effects of the cosmological constants set in (which is what we assume in the rest of this discussion relying on it being well-constrained by the CMB power spectrum), $\Lambda_{\rm s}$CDM will have a weaker antagonist term up to the redshift $z_\dagger$ due to its negative valued cosmological constant which supports structure formation by lowering $H(z > z_\dagger)$ compared to both the ΛCDM and Einstein-de Sitter (viz., ΛCDM with $\Lambda = 0$) models, consequently yielding an enhanced growth of structure at least for $z > z_\dagger$ (i.e., for $z \gtrsim 2$ according to constraints we found on $z_\dagger$ in this work).[7] If the values of the cosmological constants for both models were to be the same after the sign switch (i.e., $|\Lambda_{\rm s}| = \Lambda$) for a given $\delta_{\rm m}(z > z_\dagger)$ value for both models, this would result in enhancement in the present-day structure for $\Lambda_{\rm s}$CDM since $H(z)$ would be the same for both models for $z < z_\dagger$ while the structure supporting nature of the negative cosmological constant of $\Lambda_{\rm s}$CDM would have resulted in a greater $\delta_{\rm m}$ value at $z = z_\dagger$. However, the observational constraints on $D_M(z_*)$ require that the lower $H(z > z_\dagger)$ values of $\Lambda_{\rm s}$CDM compared to ΛCDM should be compensated by higher $H(z < z_\dagger)$ values, i.e., $|\Lambda_{\rm s}| > \Lambda$. Hence, for $z < z_\dagger$, the cosmological constant of $\Lambda_{\rm s}$CDM will have a stronger impact against growth of structures compared to ΛCDM. The answer to whether these two competing effects before and after $z_\dagger$ result in a greater present-day amplitude of growth of structure for $\Lambda_{\rm s}$CDM or not, can be reached by observational analysis, and is conceivably dependent on the value of $z_\dagger$, which controls both the value of $|\Lambda_{\rm s}|$ and the amount of time the Universe spends in the phases with negative and positive cosmological constants. Note that, a smaller $z_\dagger$ results in a greater value for $|\Lambda_{\rm s}|$ and an extended era with the negative cosmological constant, and in the $z_\dagger \to \infty$ limit, $\Lambda_{\rm s}$CDM approaches ΛCDM.

The results of the observational analyses in Tables II and III present S_8 values that are lower for $\Lambda_{\rm s}$CDM compared to ΛCDM for all six data sets except for the CMB + Pan + BAO + M_B case for which both models yield the same constraints. This is despite $\Lambda_{\rm s}$CDM yielding higher constraints on σ_8 for all cases in line with our theoretical discussion. Since the low-redshift probes find lower S_8 values compared to the predictions of ΛCDM, the tensions presented in Table IV are always lower for $\Lambda_{\rm s}$CDM except for the CMB + Pan + BAO + M_B case for which both models have the same amount of tension. For $\Lambda_{\rm s}$CDM, the inclusion of the M_B prior results in a better amelioration and the inclusion of the full BAO data has an hindering effect—note that, in contrast, addition of the M_B prior makes little to no difference for the ΛCDM model in amelioration of the S_8 discrepancy. The similarities between this discussion on the constraints and tensions of S_8 and the ones in Secs. IV A and IV B on the constraints and tensions on M_B and H_0 are unsurprising due to the strong correlations among these parameters (see Fig. 4 for the correlation between H_0 and S_8). Interestingly, Fig. 4 indicates that the simultaneous alleviation of the H_0 and S_8 tensions within $\Lambda_{\rm s}$CDM is possible if the local H_0 measurement of SH0ES is considered but not the TRGB. Finally, note that the S_8 values as measured by the low-redshift probes are not model-independent, and an absolute determination of the status of the S_8 discrepancy within $\Lambda_{\rm s}$CDM requires the analyses of the low-redshift observations with $\Lambda_{\rm s}$CDM as the underlying cosmological model.

D. BAO and Ly-α discrepancies

In all, the SDSS, BOSS, and eBOSS surveys provide galaxy and quasar samples from which BAO can be measured covering all redshifts $z < 2.2$, and Ly-α forest observations over $2 < z < 3.5$. In Table I, we list the latest BAO measurements at seven different effective redshifts ($z_{\rm eff}$), viz., $D_H/r_{\rm d}$, $D_M/r_{\rm d}$, and $D_V/r_{\rm d}$, where $D_H(z) \equiv c/H(z)$ is the Hubble distance at redshift z, $D_M(z) \equiv c\int_0^z {\rm d}z'/H(z')$ is the comoving angular diameter distance in a spatially flat Robertson-Walker (RW) spacetime, $D_V(z) = [zD_H(z)D_M^2(z)]^{1/3}$ is the spherically averaged distance, and $r_{\rm d} = \int_{z_{\rm d}}^{\infty} {\rm d}z c_{\rm s}(z)/H(z)$ is the radius of sound horizon at drag epoch ($z_{\rm d} \sim 1060$) with $c_{\rm s}(z) = c[3 + 9\rho_{\rm b}/4\rho_\gamma(z)]^{-1/2}$ being the speed of sound in the baryon-photon fluid.

There appears to be a discordance between the low- and high-redshift BAO data within ΛCDM. The Ly-α BAO measurements of $D_M(2.34)/r_{\rm d}$ and $D_H(2.34)/r_{\rm d}$ from the BOSS DR11 sample were found to be in a tension of approximately 2.5σ with the best-fit predictions of Planck CMB within ΛCDM, whereas the Galaxy BAO measurements from lower redshifts including the ones from the same sample showed no significant discrepancy [52]. Moreover, an unanchored analysis of these BAO data without the presence of additional data such as CMB, presented a tension of approximately 2.5σ with a non-evolving DE (i.e., the usual cosmological constant) for $z < 2.34$ [181]; and when DE was allowed to evolve in Ref. [52], Ly-α data showed a preference for negative DE density values around $z = 2.34$. With the final eBOSS (SDSS DR16) measurement, this tension between the Ly-α BAO and Planck CMB data is reduced to approximately 1.5σ [140]—this would also correspond to a reduction of the tension in the above mentioned unanchored analysis and preference of negative DE densities, also, it is closely related to the internal tension of high and low-redshift BAO as quantified in Ref. [169] where it was also shown to

[7] In line with this feature of the $\Lambda_{\rm s}$CDM model, the recent data from the James Webb Space Telescope seem to indicate enhanced growth of structure compared to ΛCDM at high redshifts [175–177] (see also Refs. [178–180]).

diminish with updated data releases in line with the results of the recent study in Ref. [168]. Despite the reduction in these discrepancies, the BAO anomalies are still important. As discussed in Sec. IV A, the different degeneracy directions of the high- and low-redshift BAO data in the $\Omega_m - H_0$ plane when combined with BBN constraints result in a H_0 value in agreement with the CMB prediction but in significant tension with local measurements [5]. Moreover, parametric and nonparametric reconstructions of the DE density that utilize the BAO data keep finding negative (although usually consistent with vanishing) DE densities around the Ly-α data [60,91,182] indicating a DE density that transits from negative to positive today. Also, note the parallelisms of the Ly-α and S_8 discrepancies that may indicate that the resolution of these two tensions are related; first, the S_8 constraints based on the Ly-α data and weak lensing surveys probing similar redshift scales as the Ly-α measurements agree [183], second, the weakening of the tension with recent measurements happened also for the S_8 discrepancy [139,172], and third, minimal extensions of ΛCDM that relax either of these tensions tend to exacerbate the H_0 tension [10,11].

In the analyses of both models with six different data sets, the ones that include our full BAO data have distinctive properties from the rest. For the data sets without the full BAO, both models yield similar posterior distributions (especially for the CMB + Pan data set without the M_B prior) for the baseline six free parameters of ΛCDM, whereas including the full BAO data results in slight separation of the contours (see Tables II and III and Figs. 6–11 presented in the Appendix). Regarding the derived parameters, Λ_sCDM results in significantly lower S_8 values despite its higher σ_8 parameter for all data sets except when full BAO data is included in which case both models yield very similar constraints; however, Λ_sCDM yields higher H_0 and M_B values, and a lower t_0 value compared to ΛCDM whether or not full BAO is included in the data set. Expanding the BAO data set from Ly-α to the full BAO means inclusion of the Galaxy BAO at the $z_{\rm eff} = 0.15$, 0.38, 0.51, 0.70, 0.85 and also the Quasar BAO at $z_{\rm eff} = 1.48$. The effect of the Galaxy BAO at $z_{\rm eff} = 0.38$, 0.51, 0.61 on Λ_sCDM was discussed in Ref. [89] where it was found that the preference of the Galaxy BAO data for higher $z_\dagger$ values holds the model back from working efficiently in alleviating the tensions of ΛCDM as the phenomenological difference between the two models diminishes with the increasing values of $z_\dagger$. The same observation can be made also from the analyses of the present paper where the inclusion of the full BAO data set, majority of which is galaxy BAO, results in higher $z_\dagger$ values, and hence is accompanied with a worsening in amelioration of the tensions (cf. Table IV). In Fig. 5, we give expansion histories of Λ_sCDM for the mean values of the analyses with six different data sets presented in Tables II and III. And in Table V, we quantify the concordance/discordance between the ΛCDM and Λ_sCDM models and the BAO measurements listed in Table I. For the values relevant to the Ly-α measurements at $z_{\rm eff} = 2.33$, we have considered the combined values of $D_H(2.33)/r_{\rm d} = 8.99 \pm 0.19$ and $D_M(2.33)/r_{\rm d} = 37.5 \pm 1.1$ [140].

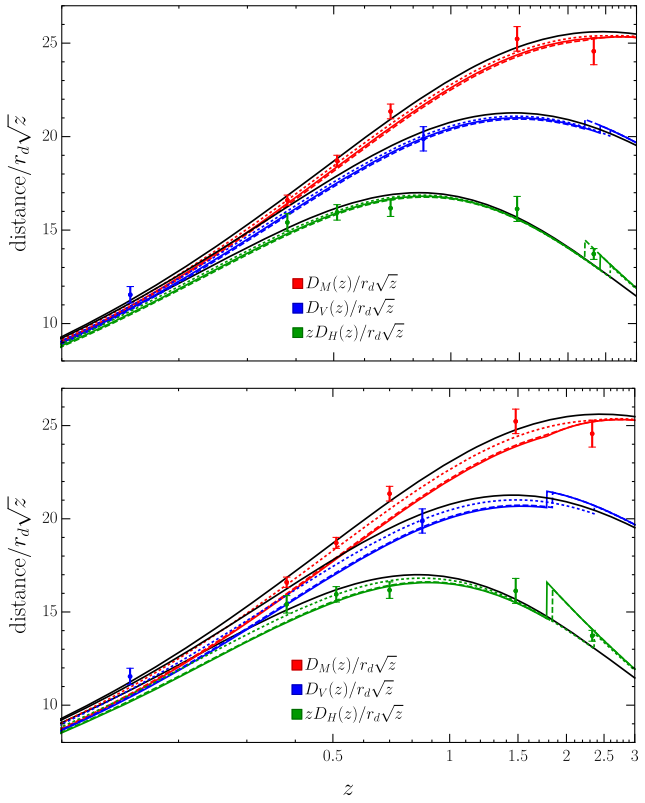

FIG. 5. Expansion histories of Λ_sCDM for the mean values of the analyses with six different data sets presented in Table II and Table III. The top and bottom panels respectively show the plots for analyses without and with the M_B prior. The solid lines are for the CMB + Pan, the dashed lines are for the CMB + Pan + Ly-α and the dotted lines are for the CMB + Pan + BAO data sets. Both the data (from Table I except we combine the Ly-α values and use $D_H(2.33)/r_{\rm d} = 8.99 \pm 0.19$ and $D_M(2.33)/r_{\rm d} = 37.5 \pm 1.1$) and the plots are color coded for different distance measures with red corresponding to $D_M(z)/r_{\rm d}\sqrt{z}$, blue to $D_V(z)/r_{\rm d}\sqrt{z}$ and green to $zD_H(z)/r_{\rm d}\sqrt{z}$. The plots for ΛCDM are given only for the CMB + Pantheon analysis without M_B as the plots for different data sets are not visually distinguishable in the figure; ΛCDM plots are all solid black and each correspond to the obvious distance measure of the branch it is closest to.

We see in Table IV that ΛCDM is typically in approximately 2σ tension with $D_H(2.33)/r_{\rm d} = 8.99 \pm 0.19$ in all cases. On the other hand, Λ_sCDM is typically fully consistent with $D_H(2.33)/r_{\rm d} = 8.99 \pm 0.19$ with the level of tension being almost zero in some cases and without exceeding 1.2σ even in the worst case. The $D_H(z)$ plots in Fig. 5 show how a $z_\dagger < 2.33$, i.e., a sign switch at smaller redshifts than the effective redshift of the Ly-α data, results in an excellent fit to the $D_H(2.33)$ measurements that is

TABLE V. Concordance/discordance between the ΛCDM and Λ_sCDM models and the BAO measurements listed in Table I. For the values relevant to the Ly-α measurements at $z_{\rm eff} = 2.33$, we have considered the combined values of $D_H(2.33)/r_d = 8.99 \pm 0.19$ and $D_M(2.33)/r_d = 37.5 \pm 1.1$ [140].

	CMB + Pan		CMB + Pan + Ly-α		CMB + Pan + BAO		CMB + Pan + M_B		CMB + Pan + Ly-α + M_B		CMB + Pan + BAO + M_B	
Data set	ΛCDM	Λ_sCDM	ΛCDM	Λ_sCDM	ΛCDM	Λ_sCDM	ΛCDM	Λ_sCDM	ΛCDM	Λ_sCDM	ΛCDM	Λ_sCDM
$D_V(0.15)/r_d$	0.9σ	1.7σ	1.0σ	1.8σ	1.0σ	0.7σ	1.2σ	2.4σ	1.3σ	2.3σ	1.2σ	1.6σ
$D_V(0.85)/r_d$	0.7σ	0.0σ	0.6σ	0.1σ	0.6σ	0.3σ	0.5σ	0.6σ	0.4σ	0.5σ	0.5σ	0.2σ
$D_M(0.38)/r_d$	0.9σ	0.6σ	0.9σ	0.9σ	0.8σ	0.2σ	0.3σ	2.0σ	0.3σ	1.8σ	0.4σ	0.3σ
$D_M(0.51)/r_d$	0.5σ	0.9σ	0.4σ	1.2σ	0.4σ	0.3σ	0.1σ	2.3σ	0.1σ	2.2σ	0.0σ	0.8σ
$D_M(0.70)/r_d$	0.9σ	1.9σ	0.9σ	2.1σ	1.0σ	1.5σ	1.3σ	3.1σ	1.4σ	3.0σ	1.3σ	2.0σ
$D_M(1.48)/r_d$	0.6σ	1.3σ	0.6σ	1.5σ	0.7σ	1.0σ	0.8σ	1.9σ	0.9σ	1.9σ	0.8σ	1.2σ
$D_M(2.33)/r_d$	1.5σ	1.0σ	1.5σ	1.0σ	1.5σ	1.2σ	1.3σ	0.9σ	1.3σ	0.9σ	1.4σ	1.1σ
$D_H(0.38)/r_d$	0.6σ	1.3σ	0.6σ	1.4σ	0.6σ	0.9σ	0.8σ	2.0σ	0.9σ	1.9σ	0.8σ	1.2σ
$D_H(0.51)/r_d$	0.7σ	0.1σ	0.6σ	0.3σ	0.6σ	0.3σ	0.4σ	0.8σ	0.4σ	0.8σ	0.4σ	0.0σ
$D_H(0.70)/r_d$	1.7σ	1.0σ	1.7σ	0.9σ	1.7σ	1.4σ	1.5σ	0.5σ	1.5σ	0.5σ	1.5σ	1.2σ
$D_H(1.48)/r_d$	0.6σ	0.8σ	0.6σ	0.8σ	0.6σ	0.7σ	0.6σ	0.9σ	0.6σ	0.9σ	0.6σ	0.8σ
$D_H(2.33)/r_d$	2.0σ	0.2σ	1.9σ	0.1σ	1.9σ	1.1σ	1.9σ	1.2σ	1.8σ	1.2σ	1.9σ	0.1σ

immediately lost for $z_\dagger > 2.33$ (also, cf. Fig. 3 in Ref. [89]). When we consider $D_M(2.33)/r_d$, both ΛCDM and Λ_sCDM models are in good consistency with $D_M(2.33)/r_d = 37.5 \pm 1.1$, yet Λ_sCDM does systematically better; while the level of tension is approximately 1.5σ in ΛCDM in all cases, it is 1σ in Λ_sCDM. The better agreement with Ly-α was expected by the theoretical and observational analyses in Ref. [89], and so was the tension with the Galaxy BAO presented in Table V. However, a careful examination of Table V exposes a characteristic of Λ_sCDM that is not present in ΛCDM; that is, in certain cases, Λ_sCDM is discrepant with the $D_M(z)/r_d$ value of a BAO measurement while it is in agreement with its $D_H(z)/r_d$ value. This is possible, since unlike $D_H(z)$, which gives information about a single instance of time, $D_M(z)$ relies on a cumulative effect from present-day up to a redshift, i.e., the integral $\int_0^z dz'/H(z')$. Thus, if the $H(z)$ of a model deviates from the actual Hubble parameter describing the Universe at low redshifts, this deviation will carry over to higher redshifts when $D_M(z)$ is considered, and can be corrected only if another deviation in the opposite direction happens (see Ref. [100] for the implications of this when $D_M(z_*)$ is considered). Moreover, since $1/H(z)$ decays rapidly with increasing z, the integral $\int_0^z dz'/H(z')$ gets most of its contribution from lower redshifts, and hence is more sensitive to deviations at low redshifts. It seems that Table V and Fig. 5 show imprints of this effect for Λ_sCDM. Let us consider the CMB + Pan + M_B case in Table V as an example since it is the one where this situation is most apparent. The tension of Λ_sCDM with the $D_M(0.70)/r_d$ measurement is at 3.1σ level whereas it is only 0.5σ for $D_H(0.70)/r_d$; this is likely to be caused by the tensions with the $D_H(z)/r_d$ values for $z < 0.5$, i.e., the 2σ tension with $D_H(0.38)/r_d$ and the 2.4σ tension with the $D_V(0.15)/r_d$ measurement, that carry over to higher redshifts for $D_M(z)/r_d$. This effect, illustrated with the above example, seems to permeate Table V, and indicates that Λ_sCDM's conflict is mainly with the BAO measurements for which $z_{\rm eff} < 0.5$, and also that the model can fit both CMB and full BAO excellently if its Hubble radius is superposed with a wavelet as discussed in Ref. [100].

E. Age discrepancy

The (present-day) age of the Universe can also be measured using very old astrophysical objects, such as globular clusters (GCs), in a cosmological model-agnostic way, in the sense that it does not depend in any significant way on the cosmological model adopted. It is estimated in Ref. [141] (see also Refs. [184,185]) that the age of the oldest GCs is $t_{\rm GC} = 13.32 \pm 0.10({\rm stat.}) \pm 0.23({\rm sys.})$ Gyr at 68% CL, which is transformed to an age of the Universe $t_{\rm u} = 13.50 \pm 0.15({\rm stat.}) \pm 0.23({\rm sys.})$ Gyr (± 0.27 when adding statistical and systematic uncertainties in quadrature). It is in good agreement with the Planck18 ΛCDM inferred age $t_0 = 13.80 \pm 0.02$ Gyr [3]. However, this

success may be due to the systematic uncertainties that are currently too large; there are ongoing efforts to reduce the impact of systematic uncertainties so that GCs' constraints on t_0 can potentially discriminate among different cosmological models, in particular, the models that are proposed to solve the H_0 tension [185,186]. When we consider the age of the Universe estimated from GCs by taking only the statistical uncertainties into account, viz., $t_u = 13.50 \pm 0.15$ Gyr at 68% CL, while the Planck18 ΛCDM finds 2σ tension, the Λ_sCDM model is expected to find an even better agreement as Λ_s reduces the age of the Universe [89]. Our results for t_0 are summarized in Table IV and Fig. 2. We see that in all three analyses without the M_B prior, ΛCDM is in tension with t_u estimated from GCs mentioned above at the level of 1.9σ, whereas the Λ_sCDM model is in tension at less than 1σ, except reaches 1.4σ tension for the CMB + Pan + BAO case. On the other hand, when the M_B prior is included in the analysis, the tensions of ΛCDM decrease only slightly to 1.7σ for all three analyses, but Λ_sCDM becomes fully consistent; even the largest tension for Λ_sCDM is just 1.1σ (CMB + Pan + BAO + M_B). Of course, to be able to conclude whether there is a real tension within ΛCDM between the age of the Universe as predicted by CMB and the one inferred from GCs, and to use t_u as a discriminator between cosmological models, we need the systematic uncertainties in t_u to be reduced. However, it is important to notice the clear correlations of the parameter $z_\dagger$ of the Λ_sCDM model with not only t_0 but also the parameters H_0, M_B, S_8, and $D_H(2.33)/r_d$ in Fig. 2. Moreover, not only the Λ_sCDM predicted t_0 values find better agreement with the one predicted by GCs, but also the Λ_sCDM predicted values of H_0, M_B, S_8, and $D_H(2.33)/r_d$ are consistent with their direct observational values. It is very difficult to simply call it a coincidence, and as systematic uncertainties are removed, it would not be a surprise if the age of the Universe turns out to be smaller than the Planck18 ΛCDM prediction.

F. ω_b discrepancy

The BBN constraints on ω_b depend on the assumed nuclear reaction rates. The most important one for deuterium destruction relevant to BBN is the $D(p,\gamma)^3$He reaction rate which was recently measured by the LUNA (The Laboratory for Underground Nuclear Astrophysics) experiment [128]. They use their measurements to give the constraint $\omega_b^{\rm LUNA} = 0.02233 \pm 0.00036$ on the physical density parameter of baryons. Using the same measurement by LUNA and a more theoretically guided approach for the two other important processes for deuterium destruction, Ref. [142] has reported the constraint $\omega_b^{\rm PCUV21} = 0.02195 \pm 0.00022$. Compared to the CMB only prediction $\omega_b = 0.02237 \pm 0.00015$ from Planck, which increases to $\omega_b = 0.02242 \pm 0.00014$ when BAO data is included [3], $\omega_b^{\rm LUNA}$ shows excellent agreement while the more theoretical value $\omega_b^{\rm PCUV21}$ presents some discrepancy. These are in line with the previous trend where predictions of CMB agree well with empirical approaches based on experimentally measured cross sections while more theoretical approaches are discrepant. See Ref. [187] where the theoretical $D(p,\gamma)^3$He rate yields $\omega_b = 0.02166 \pm 0.00019$ whereas the empirical one yields $\omega_b = 0.02235 \pm 0.00037$.

In Ref. [89], both ΛCDM and Λ_sCDM yielded similar ω_b values discrepant with theoretical BBN constraints, and inclusion of the BAO in the data set resulted in an exacerbation of this discrepancy for ΛCDM as in the analyses of Planck, but, it resulted in an amelioration for Λ_sCDM. Intrigued by these results, in this paper, we also computed the tensions of both models with both empirically and theoretically guided BBN constraints on ω_b. From Tables II and III, we see that both models yield ω_b values higher than BBN constraints. While inclusion of the M_B prior increases these values further, inclusion of the BAO data increases ω_b for ΛCDM but decreases it for Λ_sCDM pulling the extended model towards BBN constraints. When $\omega_b^{\rm LUNA}$ is considered, both models are in excellent agreement for all data sets; when $\omega_b^{\rm PCUV21}$ is considered, both models are moderately discrepant for all six data sets. However, it is worth noting that ω_b values for Λ_sCDM are lower for all data sets in better agreement with BBN constraints up to 0.5σ. Also, since the ω_b tensions within Λ_sCDM increase with the inclusion of the M_B prior and decrease with the inclusion of the full BAO data set, out of the six different discrepancies presented in Table IV, it is the only one that prefers relatively larger $z_\dagger$ values.

V. CONCLUSION

The Λ_sCDM model is based on the recent conjecture that the Universe went through a spontaneous AdS to dS transition characterized by a sign-switching cosmological constant (Λ_s) at $z \sim 2$ [68,89]. This conjecture was inspired by the promising observational findings on the gDE model that showed the gDE, which smoothly transitions from negative to positive energy densities, can simultaneously ameliorate the H_0 and Ly-α discrepancies by preferring a rapid transition at $z \sim 2$, and it was further compelled by some theoretical advantages of Λ_s over the gDE [68]. In this paper, we consider the simplest Λ_sCDM model, constructed simply by promoting the usual cosmological constant Λ of the standard ΛCDM model to an abrupt sign-switching cosmological constant Λ_s, which we treat as an idealized description of a rapid transition (may or may not be smooth) from an AdS vacuum provided by $\Lambda_s = -\Lambda_{s0}$ to a dS vacuum provided by $\Lambda_s = \Lambda_{s0}$, or DE models such as gDE, that can mimic this behavior. This model has been recently proposed in Ref. [89] and explored theoretically and observationally. It was found that, when Λ_sCDM is guaranteed to be consistent with the CMB data at the

background level, it predicts a higher H_0 value compared to ΛCDM and agrees with the Ly-α data for $z_\dagger \lesssim 2.3$. In the robust observational analyses, it was able to simultaneously ameliorate the H_0, M_B, and S_8 tensions along with the Ly-α and ω_b anomalies. However, while the CMB data alone was consistent with any $z_\dagger$ value for $z_\dagger \gtrsim 1.5$; when a compilation of BAO data was combined with the CMB data, the constraint on $z_\dagger$ turned out to be $z_\dagger \sim 2.4$, compromising the success of the model in ameliorating the tensions. This compromise was attributed to the opposition of galaxy BAO to lesser $z_\dagger$ values thereby preventing the model from achieving $z_\dagger \sim 2$ required for complete removal of the tensions under consideration, or equivalently, it was attributed to the discordance of low-redshift and high-redshift BAO within Λ_sCDM (that is also present within ΛCDM).

In this paper, we have constrained the parameters of Λ_sCDM and ΛCDM models with various combinations of updated and extended data compared to Ref. [89], with particular focus on the Pantheon SNIa data set with and without the SH0ES M_B prior. The extended analyses in the present paper let us asses how Λ_sCDM performs in the light of this extended set of cosmological observations, and further investigate the constraints on $z_\dagger$ without the full BAO data set, which exhibits internal conflicts within Λ_sCDM, similar to those in the case of ΛCDM. The results confirm the pushback from the galaxy BAO, and show that the M_B prior strongly favors Λ_sCDM as expected since the model predicts higher H_0 values and respects the internal consistency of the SH0ES H_0 measurement utilizing M_B. When the M_B prior is present without the full BAO data set, Λ_sCDM is very strongly favored over ΛCDM in Bayesian evidence with exceptional $\Delta \ln \mathcal{Z}$ values of 12.32 and 7.77 with and without the Ly-α data respectively. The inclusion of the *completed* full BAO data set in the analysis hinders the promising features of Λ_sCDM by pushing $z_\dagger$ to higher values, yet, Λ_sCDM is still strongly favored over ΛCDM in Bayesian evidence; namely, we have $\Delta \ln \mathcal{Z} = 3.23$ (CMB + Pan + BAO + M_B) in this case. It is important to observe the trend in the case of the Λ_sCDM model that, inclusion of the M_B prior without the full BAO data set simultaneously removes all the prominent discrepancies that prevail within the standard cosmological model (viz., the H_0, M_B, and S_8 tensions), as well as the t_0 anomaly, with strict constraints on $z_\dagger$, while its inclusion causes only minor improvements in the case of the ΛCDM model.

Generically, Λ_sCDM performs better for all six discrepancies of ΛCDM considered in this paper (viz., H_0, M_B, S_8, Ly-α, t_0, and ω_b discrepancies) for all six data compilations; particularly, in the case of $z_\dagger \sim 1.8$, Λ_sCDM is remarkably successful in simultaneous alleviation of these six discrepancies. In Ref. [68], the presence of an AdS to dS transition at $z_\dagger \sim 2$ was argued mainly based on the Ly-α data preferring negative DE densities at their effective redshifts greater than 2. In Ref. [89], for CMB + BAO data, it was indeed the Ly-α data that insisted on $z_\dagger \lesssim 2.3$ despite the opposition of the galaxy BAO to lower $z_\dagger$ values. Pleasantly, the results in this paper show that the presence of the M_B prior finds excellent constraints of $z_\dagger \sim 2$ ($z_\dagger \sim 1.8$ when the full BAO data is not included) even when the Ly-α data is not included, and the consequent predictions of the Λ_sCDM model efficiently address the tensions of ΛCDM that are considered in this work.

The inclusion of the full BAO data in the data set hinders the success of Λ_sCDM due to the galaxy BAO, as was the case in Ref. [89]. However, upon careful inspection, Table I hints that Λ_sCDM is only discrepant with the BAO data at $z_{\rm eff} < 0.5$ when the $D_H(z)/r_d$ measurements are considered, but these discrepancies carry over to $D_M(z)/r_d$ measurements from BAO at higher effective redshifts since deviations in $H(z)$ at small redshifts also cause deviations in $D_M(z)/r_d$ at all redshifts. If the Λ_sCDM model is to describe the present full BAO data, a wiggly modification to its Hubble function at low redshifts as suggested in Ref. [100] (see also references therein) is in order. From an alternative point of view, the present full BAO data seem to have internal conflicts between low- and high-redshift BAO data within both the ΛCDM and Λ_sCDM models; if these are due to systematics in the galaxy BAO measurements that are to be resolved in the future bringing BAO data to concordance within Λ_sCDM, this could allow Λ_sCDM to have excellent fit to all of the data considered in our analyses without suffering from the serious to mild tensions within ΛCDM (H_0, M_B, S_8, Ly-α, and t_0), in contrast, if these are due to systematics in the high-redshift BAO measurements that are to be resolved in the future bringing BAO data to concordance within ΛCDM, ΛCDM would still be discrepant with multitude of cosmological observations.

Further analyses of Λ_sCDM can be carried out by including additional data related to structure formation such as weak lensing and redshift-space distortion from Kilo-Degree Survey (KiDS) [139] and Dark Energy Survey (DES) [172], to robustly determine the model's consistency with regards to amplitude and growth of structures, and/or the most recent CMB data from the Atacama Cosmology Telescope (ACTPol) [4] and the South Pole Telescope (SPT-3G) [6] along with the Planck data. In addition, the recent Pantheon+ [188] sample includes SNIa from the Cepheid-host galaxies whose distances are calibrated by SH0ES; thus, Λ_sCDM can be analyzed using Pantheon + in combination with the SH0ES distance measurements instead of using the Pantheon sample along with the SH0ES M_B prior. Our analyses with the M_B prior suggest that, in this case, Λ_sCDM would perform better compared to ΛCDM; and thanks to the model's submission to the internal consistency of the SH0ES H_0 measurement, this better performance would also manifest itself in a high H_0 prediction in agreement with the SH0ES value. It is worth noting that a recent study reinforces this expectation by

suggesting that Pantheon + data set itself shows the presence of negative DE density at high redshifts [105].

Other future works may investigate extensions of Λ_sCDM itself. A straightforward extension of the model can be achieved by allowing nonzero spatial curvature. This scenario is particularly interesting due to the preference of positive spatial curvature on top of ΛCDM by the CMB data; since positive spatial curvature mimics cosmic strings with negative energy density in the Friedmann equation, whether this preference of a closed space by the CMB data (i.e., the Ω_k anomaly that is closely related to the A_L anomaly due to the degeneracy between the two) still exists within Λ_sCDM, which already incorporates a negative DE density at large redshifts, is worthy of investigation [189]. Alternatively, considering that Λ_sCDM's struggle with galaxy BAO data appears to be the main factor preventing it from simultaneously fitting excellently to the variety of the high precision data considered in the present work, one may extend the model by introducing wiggles (see Ref. [100] and references therein) to its Hubble function at low redshifts (that can accommodate the full BAO data) without excessive number of free parameters.

The apparently spontaneous nature of the Λ_s, or a DE density mimicking it, and also the fact that it shifts to a larger value, in particular from negative to positive, may render finding a concrete physical mechanism underlying this scenario challenging [68,89]. However, the phenomenological success of the Λ_sCDM model despite its simplicity (particularly, when the abrupt sign-switching Λ_s is considered), is highly encouraging to look for possible physical mechanisms underlying this scenario as well as their specific imprints in the sky. We treat the abrupt sign-switching transition of Λ_s defined in Eq. (1) as an idealized description of a rapid transition (may or may not be smooth) from an AdS vacuum provided by $\Lambda_s = -\Lambda_{s0}$ to a dS vacuum provided by $\Lambda_s = \Lambda_{s0}$ at/around a certain redshift, $z_\dagger$, in the late Universe—or DE models such as gDE, that can mimic/approximate this behavior. However, this begs the question of why this transition occurs at/around a certain time instance $t = t_\dagger$, corresponding to $z = z_\dagger$, in the history of the Universe. The way this question is answered may have far-reaching theoretical and even observational implications. For instance, if we take Λ_s as an approximation to a smoothly evolving dynamical DE, whose density rapidly changes sign around $z_\dagger$, then the time instance DE density passes from negative to positive, $t_\dagger$, is not different from any other time in the time evolution of the DE (determined by the continuity equation according to the EoS parameter that characterizes it), and the concerns regarding spontaneity are mitigated; in this case, the sign change in the DE density occurs simultaneously across the entire Universe. On the other hand, if we take Λ_s as a transition phenomenon (such as phase transition, spontaneous symmetry breaking, spontaneous emission, phenomena related to catastrophe theory), subtler points arise. First of all, it becomes crucial to address what critical event/condition (could be external) triggers the sign switch. While the answer would be mechanism-dependent, it is conceivable that the sign-switch occurs when a critical local energy level is reached. Assuming such a critical energy level, in a universe with perfect spatial uniformity (i.e., in a universe perfectly described by the RW spacetime metric), every point in space would reach the critical energy level at the same cosmic time instance leading to a simultaneous sign-switch at every point in space. But in reality, the Universe is not exactly uniform (spatially), but almost-exactly uniform (cf. the CMB temperature anisotropies are $\Delta T/T \sim 10^{-5}$ level, over a wide range of angular scales), therefore the sign switch must have occurred at/around slightly different comoving time instances in the slightly overdense and underdense regions (on cosmological scales), and also, in some overdense regions (viz., the regions where the structures have grown), the Λ_s must have never transitioned to the dS phase and remained in AdS phase. This could have observable consequences in the sky, which in turn can allow for new tests of Λ_sCDM and its possible underlying mechanisms. For instance, the asynchronization in $t_\dagger$ and the possibility that sign switch has never occurred in some regions may lead to specific imprints in the CMB, the clustering of galaxies etc.—taking this at face value, the effects of the sign-switch on the CMB anomalies by itself is an intriguing topic. Finally, let us comment on one more interesting point; if the sign-switching transition of the cosmological constant is triggered when, e.g., the local energy level reaches a critical value, then it may be possible to relate $t_\dagger$ (or $z_\dagger$) to some other cosmological parameters, which in turn leads to the possibility of reducing the free parameters of Λ_sCDM to that of the base ΛCDM model, a possibility that may crown the success of the Λ_sCDM model in light of the currently available observational data.

ACKNOWLEDGMENTS

The authors are grateful to the referee for valuable comments and suggestions. Ö. A. acknowledges the support by the Turkish Academy of Sciences in the scheme of the Outstanding Young Scientist Award (TÜBA-GEBİP), and the COST Action CA21136 (CosmoVerse). Ö. A. is supported in part by TUBITAK Grant No. 122F124. S. K. gratefully acknowledges support from the Science and Engineering Research Board (SERB), Govt. of India (File No. CRG/2021/004658). E. Ö. acknowledges the support by The Scientific and Technological Research Council of Turkey (TÜBİTAK) in the scheme of 2211/A National PhD Scholarship Program. J. A. V. acknowledges the support provided by FOSEC SEP-CONACYT Investigación Básica A1-S-21925, Ciencias de Frontera No. CONACYT-PRONACES/304001/202 and No. UNAM-DGAPA-PAPIIT IN117723. A. Y. is supported by Junior Research Fellowship (CSIR/UGC Ref.

No. 201610145543) from University Grants Commission, Govt. of India.

APPENDIX: TRIANGLE POSTERIORS

In this appendix we present the one- and two-dimensional (at 68% and 95% CLs) marginalized distributions of the model parameters for both models. We do not see strong correlations between $z_\dagger$ and the six baseline parameters, but these exist among $z_\dagger, H_0, M_B, S_8$, and $\Omega_{\rm m}$. Thus, triangular plots showing the joint posteriors between the parameters present extra complementary information to the tables in the main text.

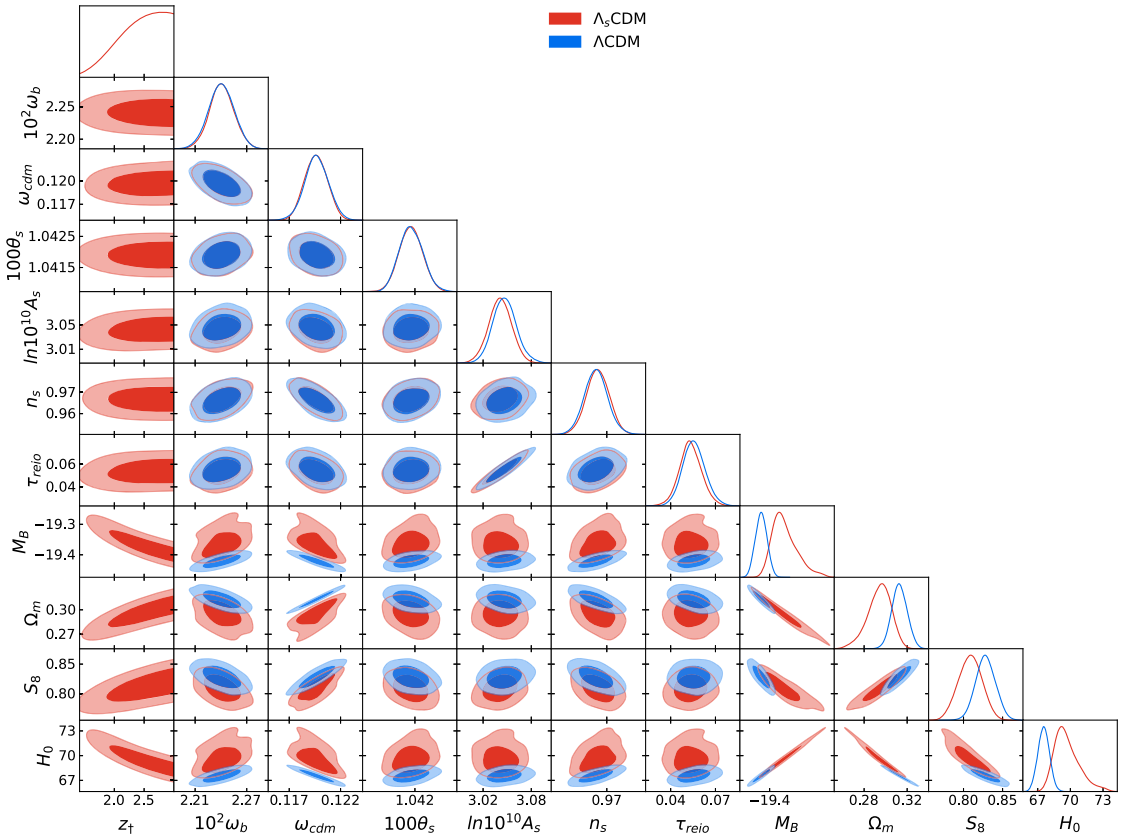

FIG. 6. One- and two-dimensional (68%, 95% CLs) marginalized distributions of the model parameters from CMB + Pan without M_B prior.

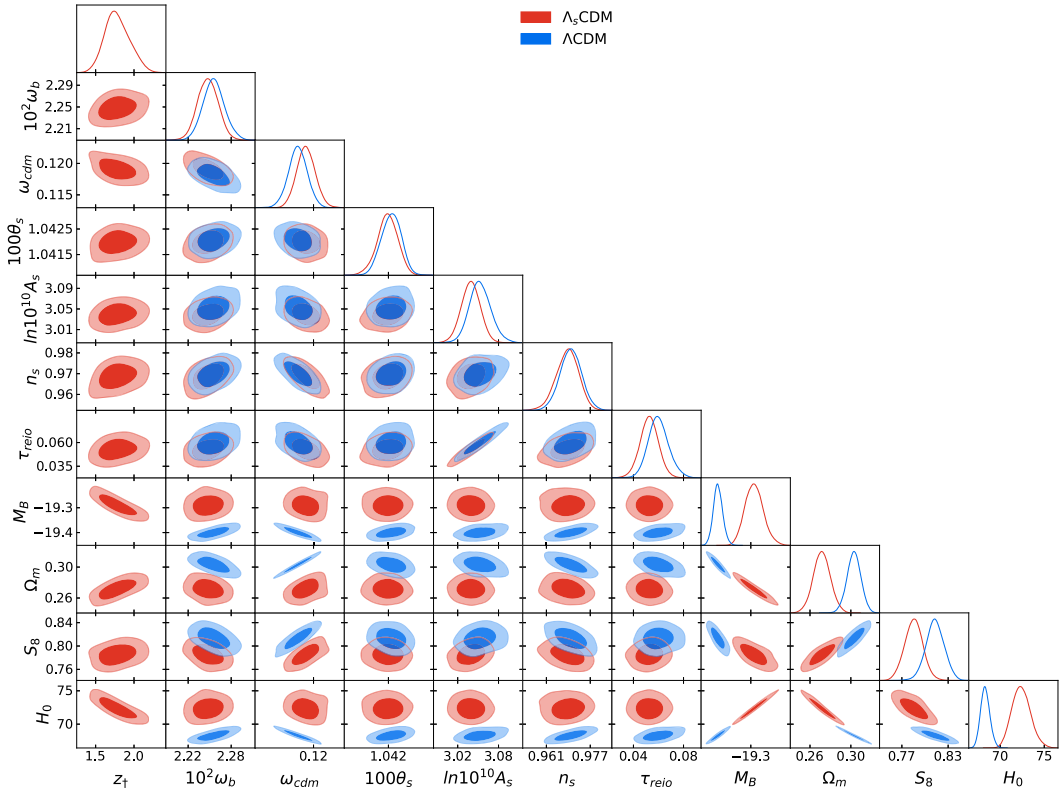

FIG. 7. One- and two-dimensional (68%, 95% CLs) marginalized distributions of the model parameters from CMB + Pan with M_B prior.

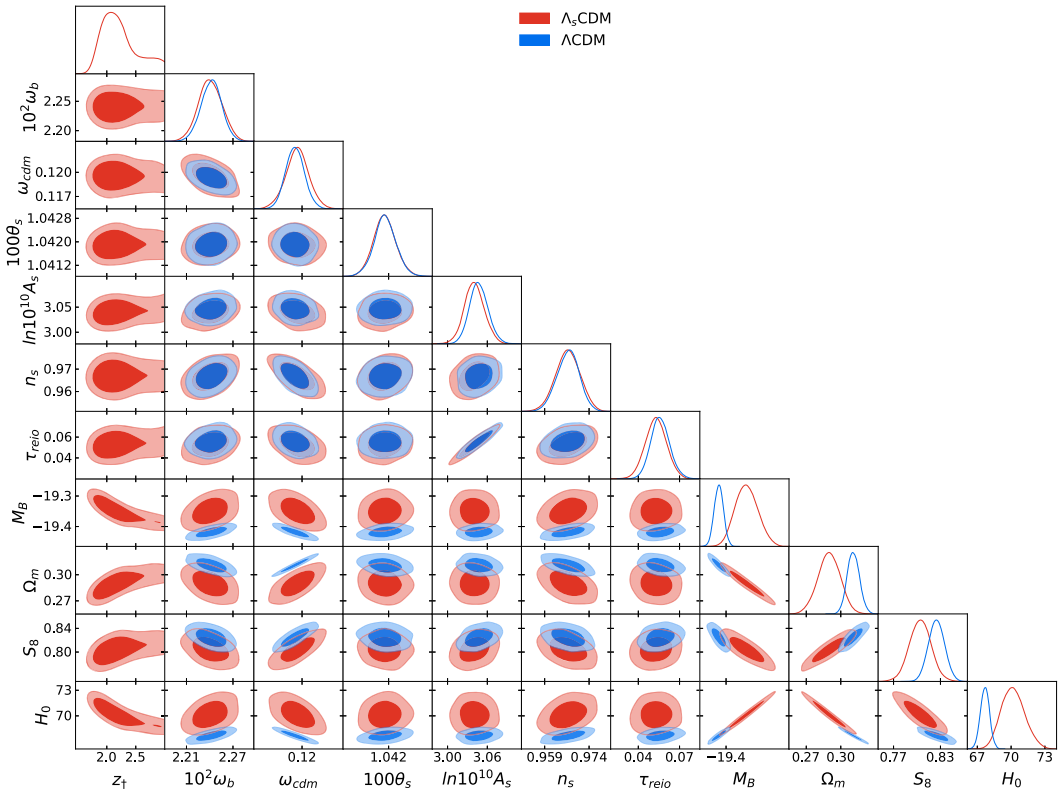

FIG. 8. One- and two-dimensional (68%, 95% CLs) marginalized distributions of the model parameters from CMB + Pan + Ly-α without M_B prior.

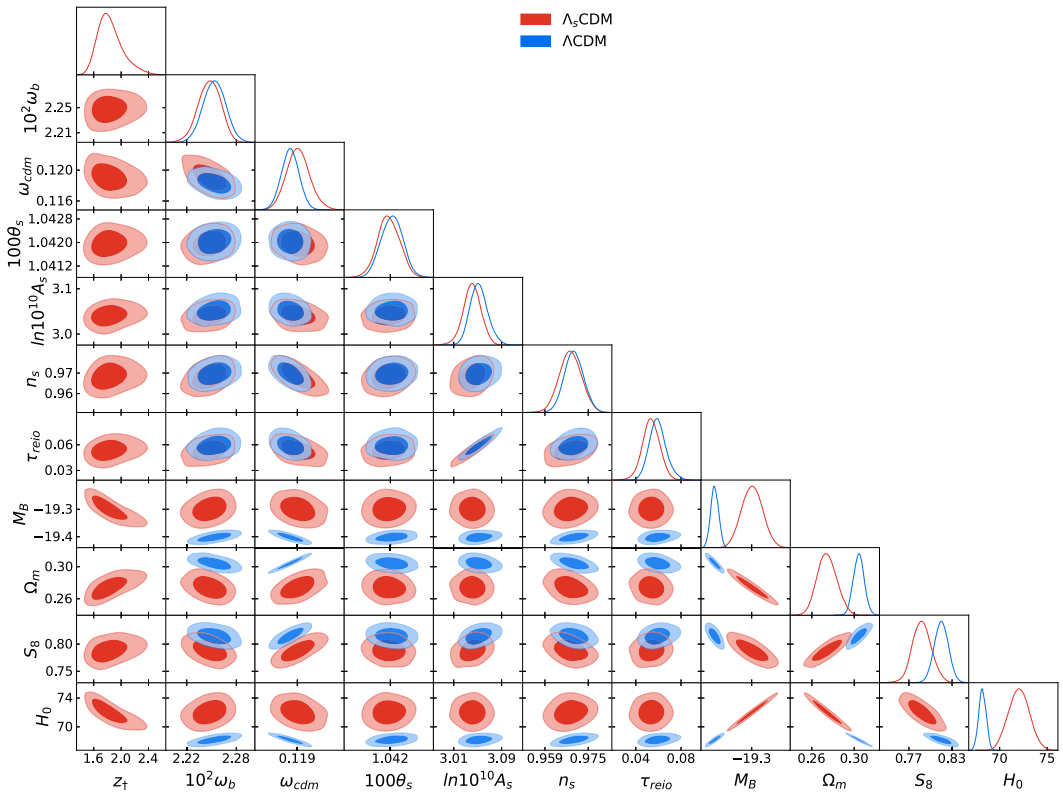

FIG. 9. One- and two-dimensional (68%, 95% CLs) marginalized distributions of the model parameters from CMB + Pan + Ly-α with M_B prior.

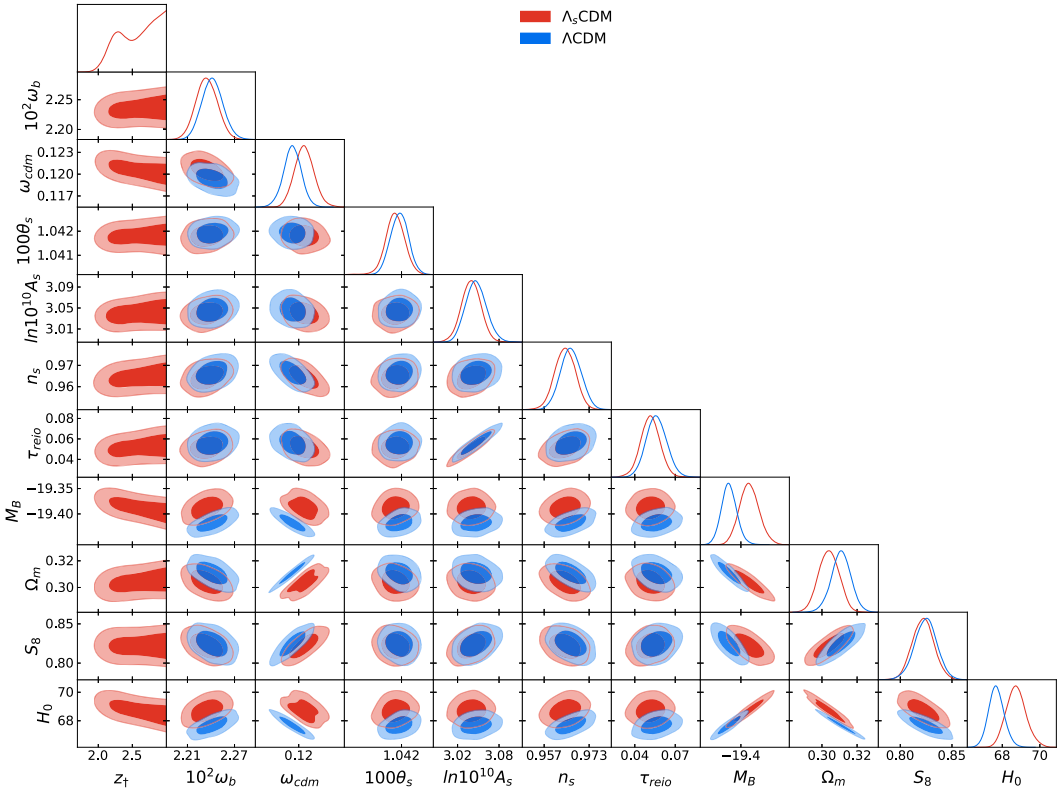

FIG. 10. One- and two-dimensional (68%, 95% CLs) marginalized distributions of the model parameters from CMB + Pan + BAO without M_B prior.

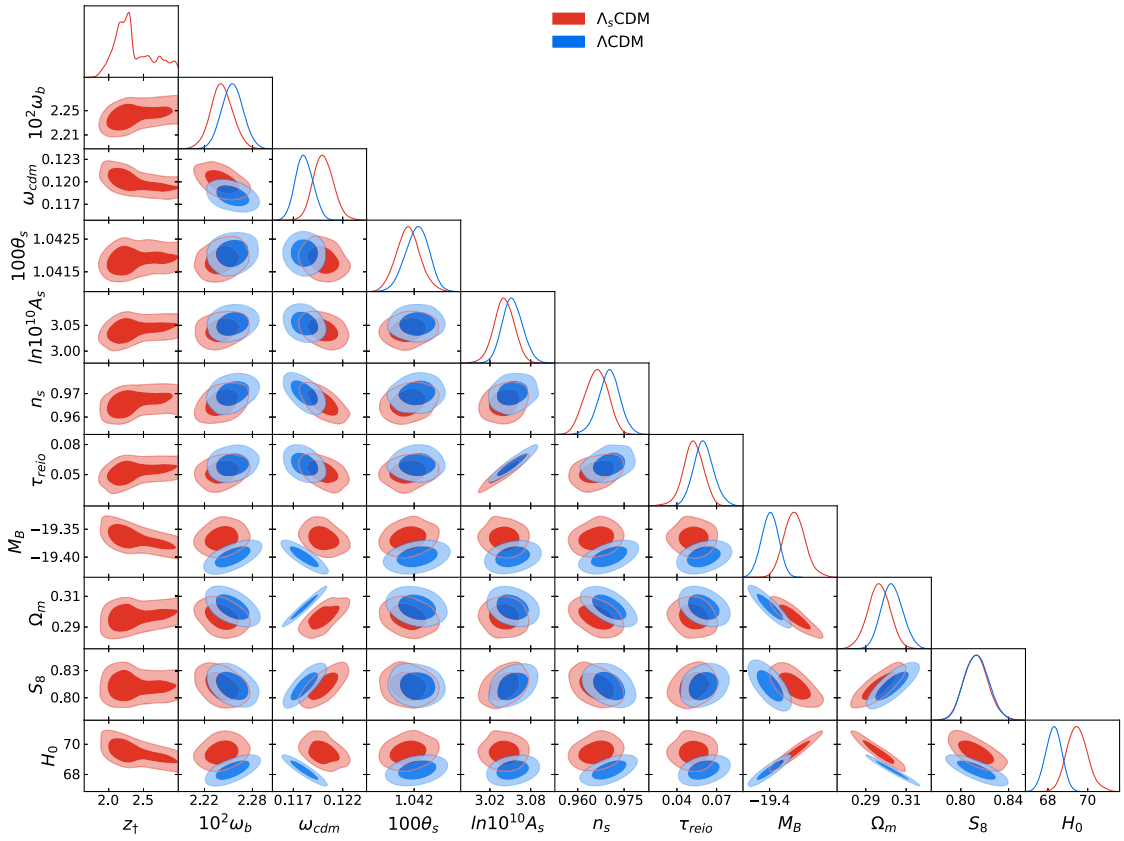

FIG. 11. One- and two-dimensional (68%, 95% CLs) marginalized distributions of the model parameters from CMB + Pan + BAO with M_B prior.

[1] A. G. Riess *et al.* (Supernova Search Team), Observational evidence from supernovae for an accelerating Universe and a cosmological constant, Astron. J. **116**, 1009 (1998).

[2] S. Perlmutter *et al.* (Supernova Cosmology Project Collaboration), Measurements of Ω and Λ from 42 high redshift supernovae, Astrophys. J. **517**, 565 (1999).

[3] N. Aghanim *et al.* (Planck Collaboration), Planck 2018 results. VI. Cosmological parameters, Astron. Astrophys. **641**, A6 (2020).

[4] S. Aiola *et al.* (ACT Collaboration), The atacama cosmology telescope: DR4 Maps and cosmological parameters, J. Cosmol. Astropart. Phys. 12 (2020) 047.

[5] S. Alam *et al.* (eBOSS Collaboration), Completed SDSS-IV extended Baryon Oscillation Spectroscopic Survey: Cosmological implications from two decades of spectroscopic surveys at the Apache Point Observatory, Phys. Rev. D **103**, 083533 (2021).

[6] L. Balkenhol *et al.* (SPT-3G Collaboration), Constraints on ΛCDM extensions from the SPT-3G 2018 EE and TE power spectra, Phys. Rev. D **104**, 083509 (2021).

[7] T. M. C. Abbott *et al.* (DES Collaboration), Dark energy survey year 3 results: Cosmological constraints from galaxy clustering and weak lensing, Phys. Rev. D **105**, 023520 (2022).

[8] T. M. C. Abbott *et al.* (DES Collaboration), Dark energy survey year 3 results: Constraints on extensions to ΛCDM with weak lensing and galaxy clustering, Phys. Rev. D **107**, 083504 (2023).

[9] E. Di Valentino, L. A. Anchordoqui, O. Akarsu, Y. Ali-Haimoud, L. Amendola, N. Arendse, M. Asgari, M. Ballardini, S. Basilakos, E. Battistelli *et al.*, Snowmass2021—Letter of interest cosmology intertwined I: Perspectives for the next decade, Astropart. Phys. **131**, 102606 (2021).

[10] E. Di Valentino, L. A. Anchordoqui, O. Akarsu, Y. Ali-Haimoud, L. Amendola, N. Arendse, M. Asgari, M. Ballardini, S. Basilakos, E. Battistelli *et al.*, Snowmass2021—Letter of interest cosmology intertwined II: The Hubble constant tension, Astropart. Phys. **131**, 102605 (2021).

[11] E. Di Valentino, L. A. Anchordoqui, Ö. Akarsu, Y. Ali-Haimoud, L. Amendola, N. Arendse, M. Asgari, M. Ballardini, S. Basilakos, E. Battistelli *et al.*, Cosmology intertwined III: $f\sigma_8$ and S_8, Astropart. Phys. **131**, 102604 (2021).

[12] E. Di Valentino, L. A. Anchordoqui, Ö. Akarsu, Y. Ali-Haimoud, L. Amendola, N. Arendse, M. Asgari, M.

Ballardini, S. Basilakos, E. Battistelli *et al.*, Snowmass2021—Letter of interest cosmology intertwined IV: The age of the universe and its curvature, Astropart. Phys. **131**, 102607 (2021).
[13] E. Di Valentino, O. Mena, S. Pan, L. Visinelli, W. Yang, A. Melchiorri, D. F. Mota, A. G. Riess, and J. Silk, In the realm of the Hubble tension—a review of solutions, Classical Quantum Gravity **38**, 153001 (2021).
[14] L. Perivolaropoulos and F. Skara, Challenges for ΛCDM: An update, New Astron. Rev. **95**, 101659 (2022).
[15] E. Abdalla, G. F. Abellán, A. Aboubrahim, A. Agnello, Ö. Akarsu, Y. Akrami, G. Alestas, D. Aloni, L. Amendola, L. A. Anchordoqui *et al.*, Cosmology intertwined: A review of the particle physics, astrophysics, and cosmology associated with the cosmological tensions and anomalies, J. High Energy Astrophys. **34**, 49 (2022).
[16] J. Annis, J. A. Newman, and A. Slosar, Snowmass2021 Cosmic frontier: Report of the CF04 topical group on dark energy and cosmic acceleration in the modern universe, arXiv:2209.08049.
[17] E. Di Valentino, W. Giarè, A. Melchiorri, and J. Silk, A health checkup test of the standard cosmological model in view of recent cosmic microwave background anisotropies experiments, Phys. Rev. D **106**, 103506 (2022).
[18] A. G. Riess, W. Yuan, L. M. Macri, D. Scolnic, D. Brout, S. Casertano, D. O. Jones, Y. Murakami, L. Breuval, T. G. Brink *et al.*, A comprehensive measurement of the local value of the Hubble constant with 1 km/s/Mpc uncertainty from the Hubble space telescope and the SH0ES team, Astrophys. J. Lett. **934**, L7 (2022).
[19] V. Poulin, T. L. Smith, T. Karwal, and M. Kamionkowski, Early Dark Energy can Resolve the Hubble Tension, Phys. Rev. Lett. **122**, 221301 (2019).
[20] T. L. Smith, V. Poulin, and M. A. Amin, Oscillating scalar fields and the Hubble tension: A resolution with novel signatures, Phys. Rev. D **101**, 063523 (2020).
[21] L. Herold and E. G. M. Ferreira, Resolving the Hubble tension with early dark energy, arXiv:2210.16296.
[22] M. Kamionkowski and A. G. Riess, The Hubble tension and early dark energy, arXiv:2211.04492.
[23] F. Niedermann and M. S. Sloth, New early dark energy, Phys. Rev. D **103**, L041303 (2021).
[24] F. Niedermann and M. S. Sloth, Resolving the Hubble tension with new early dark energy, Phys. Rev. D **102**, 063527 (2020).
[25] S. Kumar, R. C. Nunes, and S. K. Yadav, Dark sector interaction: A remedy of the tensions between CMB and LSS data, Eur. Phys. J. C **79**, 576 (2019).
[26] E. Di Valentino, A. Melchiorri, O. Mena, and S. Vagnozzi, Interacting dark energy in the early 2020s: A promising solution to the H0 and cosmic shear tensions, Phys. Dark Universe **30**, 100666 (2020).
[27] S. Kumar, Remedy of some cosmological tensions via effective phantom-like behavior of interacting vacuum energy, Phys. Dark Universe **33**, 100862 (2021).
[28] A. Bernui, E. Di Valentino, W. Giarè, S. Kumar, and R. C. Nunes, Solution of H_0 tension with evidence of dark sector interaction from 2D BAO measurements, Phys. Rev. D **107**, 103531 (2023).
[29] S. Vagnozzi, S. Dhawan, M. Gerbino, K. Freese, A. Goobar, and O. Mena, Constraints on the sum of the neutrino masses in dynamical dark energy models with $w(z) \geq -1$ are tighter than those obtained in ΛCDM, Phys. Rev. D **98**, 083501 (2018).
[30] E. Di Valentino, R. Z. Ferreira, L. Visinelli, and U. Danielsson, Late time transitions in the quintessence field and the H_0 tension, Phys. Dark Universe **26**, 100385 (2019).
[31] E. Di Valentino, A. Melchiorri, and J. Silk, Cosmological constraints in extended parameter space from the Planck 2018 legacy release, J. Cosmol. Astropart. Phys. 01 (2020) 013.
[32] A. Banerjee, H. Cai, L. Heisenberg, E.Ó. Colgáin, M. M. Sheikh-Jabbari, and T. Yang, Hubble sinks in the low-redshift swampland, Phys. Rev. D **103**, L081305 (2021).
[33] J. A. Vázquez, D. Tamayo, A. A. Sen, and I. Quiros, Bayesian model selection on scalar ϵ-field dark energy, Phys. Rev. D **103**, 043506 (2021).
[34] L. Heisenberg, H. Villarrubia-Rojo, and J. Zosso, Can late-time extensions solve the H_0 and σ_8 tensions?, Phys. Rev. D **106**, 043503 (2022).
[35] B. H. Lee, W. Lee, E. Ó. Colgáin, M. M. Sheikh-Jabbari, and S. Thakur, Is local H_0 at odds with dark energy EFT?, J. Cosmol. Astropart. Phys. 04 (2022) 004.
[36] V. Poulin, T. L. Smith, and T. Karwal, The ups and downs of early dark energy solutions to the Hubble tension: A review of models, hints and constraints circa 2023, arXiv:2302.09032.
[37] S. Goldstein, J. C. Hill, V. Iršič, and B. D. Sherwin, Canonical Hubble-tension-resolving early dark energy cosmologies are inconsistent with the Lyman-α forest, arXiv:2303.00746.
[38] G. Franco Abellán, R. Murgia, V. Poulin, and J. Lavalle, Implications of the S_8 tension for decaying dark matter with warm decay products, Phys. Rev. D **105**, 063525 (2022).
[39] Z. Davari, V. Marra, and M. Malekjani, Cosmological constrains on minimally and non-minimally coupled scalar field models, Mon. Not. R. Astron. Soc. **491**, 1920 (2020).
[40] J. Solà Peracaula, A. Gómez-Valent, J. de Cruz Pérez, and C. Moreno-Pulido, Brans–Dicke cosmology with a Λ-term: A possible solution to ΛCDM tensions, Classical Quantum Gravity **37**, 245003 (2020).
[41] J. Solà Peracaula, A. Gomez-Valent, J. de Cruz Pérez, and C. Moreno-Pulido, Brans–Dicke gravity with a cosmological constant smoothes out ΛCDM tensions, Astrophys. J. Lett. **886**, L6 (2019).
[42] S. Camera, M. Martinelli, and D. Bertacca, Does quartessence ease cosmic tensions?, Phys. Dark Universe **23**, 100247 (2019).
[43] E. Di Valentino and S. Bridle, Exploring the tension between current cosmic microwave background and cosmic shear data, Symmetry **10**, 585 (2018).
[44] R. Murgia, G. F. Abellán, and V. Poulin, Early dark energy resolution to the Hubble tension in light of weak lensing surveys and lensing anomalies, Phys. Rev. D **103**, 063502 (2021).

[45] M. Archidiacono, D. C. Hooper, R. Murgia, S. Bohr, J. Lesgourgues, and M. Viel, Constraining dark matter-dark radiation interactions with CMB, BAO, and Lyman-α, J. Cosmol. Astropart. Phys. 10 (2019) 055.
[46] A. Chudaykin, D. Gorbunov, and N. Nedelko, Exploring ΛCDM extensions with SPT-3G and Planck data: 4σ evidence for neutrino masses and implications of extended dark energy models for cosmological tensions, arXiv:2203.03666.
[47] M. Lucca, Dark energy–dark matter interactions as a solution to the S8 tension, Phys. Dark Universe **34**, 100899 (2021).
[48] J. Solà Peracaula, A. Gómez-Valent, J. de Cruz Perez, and C. Moreno-Pulido, Running vacuum against the H_0 and σ_8 tensions, Europhys. Lett. **134**, 19001 (2021).
[49] N. Khosravi and M. Farhang, Phenomenological gravitational phase transition: Early and late modifications, Phys. Rev. D **105**, 063505 (2022).
[50] G. Benevento, J. A. Kable, G. E. Addison, and C. L. Bennett, An exploration of an early gravity transition in light of cosmological tensions, Astrophys. J. **935**, 156 (2022).
[51] S. Heimersheim, N. Schöneberg, D. C. Hooper, and J. Lesgourgues, Cannibalism hinders growth: Cannibal dark matter and the S_8 tension, J. Cosmol. Astropart. Phys. 12 (2020) 016.
[52] É. Aubourg *et al.*, Cosmological implications of baryon acoustic oscillation measurements, Phys. Rev. D **92**, 123516 (2015).
[53] T. Delubac *et al.* (BOSS Collaboration), Baryon acoustic oscillations in the Lyα forest of BOSS DR11 quasars, Astron. Astrophys. **574**, A59 (2015).
[54] V. Sahni, A. Shafieloo, and A. A. Starobinsky, Model independent evidence for dark energy evolution from baryon acoustic oscillations, Astrophys. J. **793**, L40 (2014).
[55] E. Di Valentino, E. V. Linder, and A. Melchiorri, Vacuum phase transition solves the H_0 tension, Phys. Rev. D **97**, 043528 (2018).
[56] E. Mörtsell and S. Dhawan, Does the Hubble constant tension call for new physics?, J. Cosmol. Astropart. Phys. 09 (2018) 025.
[57] V. Poulin, K. K. Boddy, S. Bird, and M. Kamionkowski, Implications of an extended dark energy cosmology with massive neutrinos for cosmological tensions, Phys. Rev. D **97**, 123504 (2018).
[58] J. A. Vazquez, S. Hee, M. P. Hobson, A. N. Lasenby, M. Ibison, and M. Bridges, Observational constraints on conformal time symmetry, missing matter and double dark energy, J. Cosmol. Astropart. Phys. 07 (2018) 062.
[59] S. Capozziello, Ruchika, and A. A. Sen, Model-independent constraints on dark energy evolution from low-redshift observations, Mon. Not. R. Astron. Soc. **484**, 4484 (2019).
[60] Y. Wang, L. Pogosian, G. B. Zhao, and A. Zucca, Evolution of dark energy reconstructed from the latest observations, Astrophys. J. Lett. **869**, L8 (2018).
[61] A. Banihashemi, N. Khosravi, and A. H. Shirazi, Phase transition in the dark sector as a proposal to lessen cosmological tensions, Phys. Rev. D **101**, 123521 (2020).
[62] K. Dutta, Ruchika, A. Roy, A. A. Sen, and M. M. Sheikh-Jabbari, Beyond ΛCDM with low and high redshift data: implications for dark energy, Gen. Relativ. Gravit. **52**, 15 (2020).
[63] A. Banihashemi, N. Khosravi, and A. H. Shirazi, Ginzburg-Landau theory of dark energy: A framework to study both temporal and spatial cosmological tensions simultaneously, Phys. Rev. D **99**, 083509 (2019).
[64] Ö. Akarsu, N. Katırcı, N. Özdemir, and J. A. Vázquez, Anisotropic massive Brans-Dicke gravity extension of the standard ΛCDM model, Eur. Phys. J. C **80**, 32 (2020).
[65] Ö. Akarsu, J. D. Barrow, C. V. R. Board, N. M. Uzun, and J. A. Vazquez, Screening Λ in a new modified gravity model, Eur. Phys. J. C **79**, 846 (2019).
[66] S. Vagnozzi, New physics in light of the H_0 tension: An alternative view, Phys. Rev. D **102**, 023518 (2020).
[67] L. Visinelli, S. Vagnozzi, and U. Danielsson, Revisiting a negative cosmological constant from low-redshift data, Symmetry **11**, 1035 (2019).
[68] Ö. Akarsu, J. D. Barrow, L. A. Escamilla, and J. A. Vazquez, Graduated dark energy: Observational hints of a spontaneous sign switch in the cosmological constant, Phys. Rev. D **101**, 063528 (2020).
[69] G. Ye and Y. Piao, Is the Hubble tension a hint of AdS phase around recombination?, Phys. Rev. D **101**, 083507 (2020).
[70] X. Li and A. Shafieloo, Evidence for emergent dark energy, Astrophys. J. **902**, 58 (2020).
[71] A. Perez, D. Sudarsky, and E. Wilson-Ewing, Resolving the H_0 tension with diffusion, Gen. Relativ. Gravit. **53**, 7 (2021).
[72] A. Chavda, J. D. Barrow, and C. G. Tsagas, Kinematical and dynamical aspects of ghost-matter cosmologies, Classical Quantum Gravity **37**, 205010 (2020).
[73] Ö. Akarsu, N. Katırcı, S. Kumar, R. C. Nunes, B. Öztürk, and S. Sharma, Rastall gravity extension of the standard ΛCDM model: Theoretical features and observational constraints, Eur. Phys. J. C **80**, 1050 (2020).
[74] R. Calderón, R. Gannouji, B. L'Huillier, and D. Polarski, Negative cosmological constant in the dark sector?, Phys. Rev. D **103**, 023526 (2021).
[75] G. Ye and Y. S. Piao, T_0 censorship of early dark energy and AdS vacua, Phys. Rev. D **102**, 083523 (2020).
[76] Ö. Akarsu, J. D. Barrow, and N. M. Uzun, Screening anisotropy via energy-momentum squared gravity: ΛCDM model with hidden anisotropy, Phys. Rev. D **102**, 124059 (2020).
[77] F. X. Linares Cedeño and U. Nucamendi, Revisiting cosmological diffusion models in unimodular gravity and the H_0 tension, Phys. Dark Universe **32**, 100807 (2021).
[78] A. Paliathanasis and G. Leon, Dynamics of a two scalar field cosmological model with phantom terms, Classical Quantum Gravity **38**, 075013 (2021).
[79] E. Di Valentino, A combined analysis of the H_0 late time direct measurements and the impact on the dark energy sector, Mon. Not. R. Astron. Soc. **502**, 2065 (2021).
[80] C. Krishnan, E. Ó. Colgáin, M. M. Sheikh-Jabbari, and T. Yang, Running Hubble tension and a H0 diagnostic, Phys. Rev. D **103**, 103509 (2021).

[81] A. Bonilla, S. Kumar, and R. C. Nunes, Measurements of H_0 and reconstruction of the dark energy properties from a model-independent joint analysis, Eur. Phys. J. C **81**, 127 (2021).
[82] M. Farhang and N. Khosravi, Phenomenological gravitational phase transition: Reconciliation between the late and early universe, Phys. Rev. D **103**, 083523 (2021).
[83] A. Banihashemi, N. Khosravi, and A. Shafieloo, Dark energy as a critical phenomenon: A hint from Hubble tension, J. Cosmol. Astropart. Phys. 06 (2021) 003.
[84] W. Yang, E. Di Valentino, S. Pan, A. Shafieloo, and X. Li, Generalized emergent dark energy model and the Hubble constant tension, Phys. Rev. D **104**, 063521 (2021).
[85] G. Acquaviva, Akarsu, N. Katırcı, and J. Alberto Vazquez, Simple-graduated dark energy and spatial curvature, Phys. Rev. D **104**, 023505 (2021).
[86] Z. Zhou, G. Liu, Y. Mu, and L. Xu, Can phantom transition at $z \sim 1$ restore the Cosmic concordance?, Mon. Not. R. Astron. Soc. **511**, 595 (2022).
[87] F. X. Linares Cedeño, N. Roy, and L. A. Ureña-López, Tracker phantom field and a cosmological constant: Dynamics of a composite dark energy model, arXiv:2105.07103.
[88] S. Bag, V. Sahni, A. Shafieloo, and Y. Shtanov, Phantom braneworld and the Hubble tension, Astrophys. J. **923**, 212 (2021).
[89] Ö. Akarsu, S. Kumar, E. Özülker, and J. A. Vazquez, Relaxing cosmological tensions with a sign switching cosmological constant, Phys. Rev. D **104**, 123512 (2021).
[90] N. Cruz, E. González, and J. Jovel, Singularities and soft-Big Bang in a viscous ΛCDM model, Phys. Rev. D **105**, 024047 (2022).
[91] L. A. Escamilla and J. A. Vazquez, Model selection applied to reconstructions of the dark energy, Eur. Phys. J. C **83**, 251 (2023).
[92] A. A. Sen, S. A. Adil, and S. Sen, Do cosmological observations allow a negative Λ?, Mon. Not. R. Astron. Soc. **518**, 1098 (2023).
[93] H. Wang and Y. S. Piao, Testing dark energy after pre-recombination early dark energy, Phys. Lett. B **832**, 137244 (2022).
[94] J. Q. Jiang and Y. S. Piao, Toward early dark energy and ns = 1 with Planck, ACT, and SPT observations, Phys. Rev. D **105**, 103514 (2022).
[95] G. Acquaviva and N. Katirci, Dynamical analysis of logarithmic energy-momentum squared gravity, Phys. Dark Universe **38**, 101128 (2022).
[96] E. Özülker, Is the dark energy equation of state parameter singular?, Phys. Rev. D **106**, 063509 (2022).
[97] S. S. Xue, Massive particle pair production and oscillation in Friedman Universe: its effect on inflation, Eur. Phys. J. C **83**, 267 (2023).
[98] A. A. Saharian, R. M. Avagyan, E. R. B. de Mello, V. K. Kotanjyan, T. A. Petrosyan, and H. G. Babujyan, Cosmological evolution with negative energy densities, Astrophysics **65**, 427 (2022).
[99] S. Di Gennaro and Y. C. Ong, Sign switching dark energy from a running barrow entropy, Universe **8**, 541 (2022).
[100] Ö. Akarsu, E. Ó. Colgáin, E. Özülker, S. Thakur, and L. Yin, The inevitable manifestation of wiggles in the expansion of the late universe, Phys. Rev. D **107**, 123526 (2023).
[101] H. Moshafi, H. Firouzjahi, and A. Talebian, Multiple transitions in vacuum dark energy and H_0 tension, Astrophys. J. **940**, 121 (2022).
[102] H. Wang and Y. s. Piao, A fraction of dark matter fading with early dark energy?, arXiv:2209.09685.
[103] E. Ó. Colgáin, M. M. Sheikh-Jabbari, and R. Solomon, High redshift ΛCDM cosmology: To bin or not to bin?, arXiv:2211.02129.
[104] Y. C. Ong, An effective sign switching dark energy: Lotka-Volterra model of two interacting fluids, arXiv:2212.04429.
[105] M. Malekjani, R. M. Conville, E. Ó. Colgáin, S. Pourojaghi, and M. M. Sheikh-Jabbari, Negative dark energy density from high redshift Pantheon + supernovae, arXiv:2301.12725.
[106] S. A. Adil, Ö. Akarsu, E. Di Valentino, R. C. Nunes, E. Özülker, A. A. Sen, and E. Specogna, Omnipotent dark energy: A phenomenological answer to the Hubble tension, arXiv:2306.08046.
[107] E. Di Valentino, A. Melchiorri, and J. Silk, Investigating cosmic discordance, Astrophys. J. Lett. **908**, L9 (2021).
[108] A. Semenaite, A. G. Sánchez, A. Pezzotta, J. Hou, A. Eggemeier, M. Crocce, C. Zhao, J. R. Brownstein, G. Rossi, and D. P. Schneider, Beyond ΛCDM constraints from the full shape clustering measurements from BOSS and eBOSS, Mon. Not. R. Astron. Soc. **521**, 5013 (2023).
[109] W. Handley, Curvature tension: Evidence for a closed universe, Phys. Rev. D **103**, L041301 (2021).
[110] E. Di Valentino, A. Melchiorri, and J. Silk, Planck evidence for a closed Universe and a possible crisis for cosmology, Nat. Astron. **4**, 196 (2020).
[111] S. Vagnozzi, E. Di Valentino, S. Gariazzo, A. Melchiorri, O. Mena, and J. Silk, The galaxy power spectrum take on spatial curvature and cosmic concordance, Phys. Dark Universe **33**, 100851 (2021).
[112] S. Dhawan, J. Alsing, and S. Vagnozzi, Non-parametric spatial curvature inference using late-Universe cosmological probes, Mon. Not. R. Astron. Soc. **506**, L1 (2021).
[113] J. E. Gonzalez, M. Benetti, R. von Marttens, and J. Alcaniz, Testing the consistency between cosmological data: The impact of spatial curvature and the dark energy EoS, J. Cosmol. Astropart. Phys. 11 (2021) 060.
[114] Ö. Akarsu, E. Di Valentino, S. Kumar, M. Özyiğit, and S. Sharma, Testing spatial curvature and anisotropic expansion on top of the ΛCDM model, Phys. Dark Universe **39**, 101162 (2023).
[115] E. Ó. Colgáin, M. M. Sheikh-Jabbari, R. Solomon, M. G. Dainotti, and D. Stojkovic, Putting flat ΛCDM in the (Redshift) bin, arXiv:2206.11447.
[116] W. Yang, W. Giarè, S. Pan, E. Di Valentino, A. Melchiorri, and J. Silk, Revealing the effects of curvature on the cosmological models, Phys. Rev. D **107**, 063509 (2023).
[117] E. Calabrese, A. Slosar, A. Melchiorri, G. F. Smoot, and O. Zahn, Cosmic microwave weak lensing data as a test for the dark universe, Phys. Rev. D **77**, 123531 (2008).
[118] W. L. Freedman *et al.*, The Carnegie-Chicago Hubble program. VIII. An independent determination of the Hubble constant based on the tip of the red giant branch, Astrophys. J. **882**, 34 (2019).

[119] V. Sahni and Y. Shtanov, Brane world models of dark energy, J. Cosmol. Astropart. Phys. 11 (2003) 014.
[120] V. Sahni and Y. Shtanov, Did the Universe loiter at high redshifts?, Phys. Rev. D **71**, 084018 (2005).
[121] S. Tsujikawa, K. Uddin, S. Mizuno, R. Tavakol, and J. Yokoyama, Constraints on scalar-tensor models of dark energy from observational and local gravity tests, Phys. Rev. D **77**, 103009 (2008).
[122] S. Y. Zhou, E. J. Copeland, and P. M. Saffin, Cosmological constraints on $f(G)$ dark energy models, J. Cosmol. Astropart. Phys. 07 (2009) 009.
[123] F. Bauer, J. Sola, and H. Stefancic, Dynamically avoiding fine-tuning the cosmological constant: The 'Relaxed Universe', J. Cosmol. Astropart. Phys. 12 (2010) 029.
[124] D. Camarena and V. Marra, On the use of the local prior on the absolute magnitude of Type Ia supernovae in cosmological inference, Mon. Not. R. Astron. Soc. **504**, 5164 (2021).
[125] A. G. Riess *et al.*, A 2.4% determination of the local value of the Hubble constant, Astrophys. J. **826**, 56 (2016).
[126] W. L. Freedman, Measurements of the Hubble constant: Tensions in perspective, Astrophys. J. **919**, 16 (2021).
[127] M. Blomqvist *et al.*, Baryon acoustic oscillations from the cross-correlation of Lyα absorption and quasars in eBOSS DR14, Astron. Astrophys. **629**, A86 (2019).
[128] V. Mossa, K. Stöckel, F. Cavanna, F. Ferraro, M. Aliotta, F. Barile, D. Bemmerer, A. Best, A. Boeltzig, C. Broggini *et al.*, The baryon density of the Universe from an improved rate of deuterium burning, Nature (London) **587**, 210 (2020).
[129] Ö. Akarsu, S. Kumar, E. Özülker, and A. Yadav, Family of ΛCDM cosmologies (to be published).
[130] Planck Collaboration, Planck 2018 results-V. CMB power spectra and likelihoods, Astron. Astrophys. **641**, A5 (2020).
[131] Planck Collaboration, Planck 2018 results -VIII. Gravitational lensing, Astron. Astrophys. **641**, A8 (2020).
[132] D. M. Scolnic *et al.*, The complete light-curve sample of spectroscopically confirmed Type Ia supernovae from Pan-STARRS1 and cosmological constraints from the combined Pantheon sample, Astrophys. J. **859**, 101 (2018).
[133] D. Blas, J. Lesgourgues, and T. Tram, The cosmic linear anisotropy solving system (CLASS). Part II: Approximation schemes, J. Cosmol. Astropart. Phys. 07 (2011) 034.
[134] B. Audren, J. Lesgourgues, K. Benabed, and S. Prunet, Conservative constraints on early cosmology with MONTE PYTHON, J. Cosmol. Astropart. Phys. 02 (2013) 001.
[135] MCEvidence is publicly available online at https://github.com/yabebalFantaye/MCEvidence.
[136] J. A. Vazquez, A. N. Lasenby, M. Bridges, and M. P. Hobson, A Bayesian study of the primordial power spectrum from a novel closed universe model, Mon. Not. R. Astron. Soc. **422**, 1948 (2012).
[137] L. E. Padilla, L. O. Tellez, L. A. Escamilla, and J. A. Vazquez, Cosmological parameter inference with Bayesian statistics, Universe **7**, 213 (2021).
[138] R. E. Kass and A. E. Raftery, Bayes factors, J. Am. Stat. Assoc. **90**, 773 (1995).
[139] C. Heymans, T. Tröster, M. Asgari, C. Blake, H. Hildebrandt, B. Joachimi, K. Kuijken, C. A. Lin, A. G. Sánchez, J. L. van den Busch *et al.*, KiDS-1000 cosmology: Multi-probe weak gravitational lensing and spectroscopic galaxy clustering constraints, Astron. Astrophys. **646**, A140 (2021).
[140] H. du Mas des Bourboux *et al.*, The completed SDSS-IV extended Baryon Oscillation Spectroscopic Survey: Baryon acoustic oscillations with Lyα forests, Astrophys. J. **901**, 153 (2020).
[141] D. Valcin, R. Jimenez, L. Verde, J. L. Bernal, and B. D. Wandelt, The age of the Universe with globular clusters: Reducing systematic uncertainties, J. Cosmol. Astropart. Phys. 08 (2021) 017.
[142] C. Pitrou, A. Coc, J. P. Uzan, and E. Vangioni, A new tension in the cosmological model from primordial deuterium?, Mon. Not. R. Astron. Soc. **502**, 2474 (2021).
[143] C. D. Huang, A. G. Riess, W. Yuan, L. M. Macri, N. L. Zakamska, S. Casertano, P. A. Whitelock, S. L. Hoffmann, A. V. Filippenko, and D. Scolnic, Hubble space telescope observations of mira variables in the Type Ia Supernova host NGC 1559: An alternative candle to measure the Hubble constant, Astrophys. J. **889**, 5 (2020).
[144] J. P. Blakeslee, J. B. Jensen, C. P. Ma, P. A. Milne, and J. E. Greene, The Hubble Constant from infrared surface brightness fluctuation distances, Astrophys. J. **911**, 65 (2021).
[145] P. Garnavich, C. M. Wood, P. Milne, J. B. Jensen, J. P. Blakeslee, P. J. Brown, D. Scolnic, B. Rose, and D. Brout, Connecting infrared surface brightness fluctuation distances to Type Ia Supernova hosts: Testing the top rung of the distance ladder, arXiv:2204.12060.
[146] T. de Jaeger, L. Galbany, A. G. Riess, B. E. Stahl, B. J. Shappee, A. V. Filippenko, and W. Zheng, A 5 per cent measurement of the Hubble–Lemaître constant from Type II supernovae, Mon. Not. R. Astron. Soc. **514**, 4620 (2022).
[147] D. W. Pesce, J. A. Braatz, M. J. Reid, A. G. Riess, D. Scolnic, J. J. Condon, F. Gao, C. Henkel, C. M. V. Impellizzeri, C. Y. Kuo *et al.*, The megamaser cosmology project. XIII. Combined Hubble constant constraints, Astrophys. J. Lett. **891**, L1 (2020).
[148] E. Kourkchi, R. B. Tully, G. S. Anand, H. M. Courtois, A. Dupuy, J. D. Neill, L. Rizzi, and M. Seibert, Cosmicflows-4: The calibration of optical and infrared Tully–Fisher relations, Astrophys. J. **896**, 3 (2020).
[149] D. Fernández Arenas, E. Terlevich, R. Terlevich, J. Melnick, R. Chávez, F. Bresolin, E. Telles, M. Plionis, and S. Basilakos, An independent determination of the local Hubble constant, Mon. Not. R. Astron. Soc. **474**, 1250 (2018).
[150] S. Birrer, M. Millon, D. Sluse, A. J. Shajib, F. Courbin, L. V. E. Koopmans, S. H. Suyu, and T. Treu, Time-delay cosmography: Measuring the Hubble constant and other cosmological parameters with strong gravitational lensing, arXiv:2210.10833.
[151] M. Moresco, L. Amati, L. Amendola, S. Birrer, J. P. Blakeslee, M. Cantiello, A. Cimatti, J. Darling, M. Della Valle, M. Fishbach *et al.*, Unveiling the Universe with emerging cosmological probes, Living Rev. Relativity **25**, 6 (2022).

[152] S. Refsdal, On the possibility of determining Hubble's parameter and the masses of galaxies from the gravitational lens effect, Mon. Not. R. Astron. Soc. **128**, 307 (1964).
[153] K. C. Wong, S. H. Suyu, G. C. F. Chen, C. E. Rusu, M. Millon, D. Sluse, V. Bonvin, C. D. Fassnacht, S. Taubenberger, M. W. Auger *et al.*, H0LiCOW—XIII. A 2.4 per cent measurement of H0 from lensed quasars: 5.3σ tension between early- and late-Universe probes, Mon. Not. R. Astron. Soc. **498**, 1420 (2020).
[154] M. Millon, A. Galan, F. Courbin, T. Treu, S. H. Suyu, X. Ding, S. Birrer, G. C. F. Chen, A. J. Shajib, D. Sluse *et al.*, TDCOSMO. I. An exploration of systematic uncertainties in the inference of H_0 from time-delay cosmography, Astron. Astrophys. **639**, A101 (2020).
[155] S. Birrer, A. J. Shajib, A. Galan, M. Millon, T. Treu, A. Agnello, M. Auger, G. C. F. Chen, L. Christensen, T. Collett *et al.*, TDCOSMO—IV. Hierarchical time-delay cosmography—joint inference of the Hubble constant and galaxy density profiles, Astron. Astrophys. **643**, A165 (2020).
[156] A. J. Shajib, P. Mozumdar, G. C. F. Chen, T. Treu, M. Cappellari, S. Knabel, S. H. Suyu, V. N. Bennert, J. A. Frieman, D. Sluse *et al.*, TDCOSMO. XII. Improved Hubble constant measurement from lensing time delays using spatially resolved stellar kinematics of the lens galaxy, Astron. Astrophys. **673**, A9 (2023).
[157] G. Alestas, L. Kazantzidis, and L. Perivolaropoulos, $w-M$ phantom transition at $z_t < 0.1$ as a resolution of the Hubble tension, Phys. Rev. D **103**, 083517 (2021).
[158] G. Alestas, D. Camarena, E. Di Valentino, L. Kazantzidis, V. Marra, S. Nesseris, and L. Perivolaropoulos, Late-transition versus smooth H(z)-deformation models for the resolution of the Hubble crisis, Phys. Rev. D **105**, 063538 (2022).
[159] V. Marra and L. Perivolaropoulos, Rapid transition of $G_{\rm eff}$ at $z_t \simeq 0.01$ as a possible solution of the Hubble and growth tensions, Phys. Rev. D **104**, L021303 (2021).
[160] G. Efstathiou, To H_0 or not to H_0?, Mon. Not. R. Astron. Soc. **505**, 3866 (2021).
[161] D. Camarena and V. Marra, Local determination of the Hubble constant and the deceleration parameter, Phys. Rev. Res. **2**, 013028 (2020).
[162] D. Camarena and V. Marra, On the use of the local prior on the absolute magnitude of Type Ia supernovae in cosmological inference, Mon. Not. R. Astron. Soc. **504**, 5164 (2021).
[163] G. Benevento, W. Hu, and M. Raveri, Can late dark energy transitions raise the Hubble constant?, Phys. Rev. D **101**, 103517 (2020).
[164] R. G. Cai, Z. K. Guo, S. J. Wang, W. W. Yu, and Y. Zhou, No-go guide for the Hubble tension: Late-time solutions, Phys. Rev. D **105**, L021301 (2022).
[165] K. L. Greene and F. Y. Cyr-Racine, Hubble distancing: Focusing on distance measurements in cosmology, J. Cosmol. Astropart. Phys. 06 (2022) 002.
[166] D. Benisty, J. Mifsud, J. L. Said, and D. Staicova, On the robustness of the constancy of the Supernova absolute magnitude: Non-parametric reconstruction & Bayesian approaches, arXiv:2202.04677.
[167] R. I. Anderson, N. W. Koblischke, and L. Eyer, Reconciling astronomical distance scales with variable red giant stars, arXiv:2303.04790.
[168] N. Schöneberg, L. Verde, H. Gil-Marín, and S. Brieden, BAO + BBN revisited—Growing the Hubble tension with a 0.7 km/s/Mpc constraint, J. Cosmol. Astropart. Phys. 11 (2022) 039.
[169] A. Cuceu, J. Farr, P. Lemos, and A. Font-Ribera, Baryon acoustic oscillations and the Hubble constant: Past, present and future, J. Cosmol. Astropart. Phys. 10 (2019) 044.
[170] N. Schöneberg, J. Lesgourgues, and D. C. Hooper, The BAO + BBN take on the Hubble tension, J. Cosmol. Astropart. Phys. 10 (2019) 029.
[171] D. Camarena and V. Marra, A new method to build the (inverse) distance ladder, Mon. Not. R. Astron. Soc. **495**, 2630 (2020).
[172] L. F. Secco *et al.* (DES Collaboration), Dark energy survey year 3 results: Cosmology from cosmic shear and robustness to modeling uncertainty, Phys. Rev. D **105**, 023515 (2022).
[173] T. Hamana, M. Shirasaki, S. Miyazaki, C. Hikage, M. Oguri, S. More, R. Armstrong, A. Leauthaud, R. Mandelbaum, H. Miyatake *et al.*, Cosmological constraints from cosmic shear two-point correlation functions with HSC survey first-year data, Publ. Astron. Soc. Jpn. **72**, 16 (2020); **74**, 488(E) (2022).
[174] P. J. E. Peebles, *The Large Scale Structure of the Universe* (Princeton University Press, Princeton, NJ, 1980).
[175] M. Boylan-Kolchin, Stress testing ΛCDM with high-redshift galaxy candidates, Nat. Astron. **7**, 731 (2023).
[176] C. C. Lovell, I. Harrison, Y. Harikane, S. Tacchella, and S. M. Wilkins, Extreme value statistics of the halo and stellar mass distributions at high redshift: Are JWST results in tension with ΛCDM?, Mon. Not. R. Astron. Soc. **518**, 2511 (2023).
[177] M. Haslbauer, P. Kroupa, A. H. Zonoozi, and H. Haghi, Has JWST already falsified dark-matter-driven galaxy formation?, Astrophys. J. Lett. **939**, L31 (2022).
[178] C. L. Steinhardt, P. Capak, D. Masters, and J. S. Speagle, The impossibly early galaxy problem, Astrophys. J. **824**, 21 (2016).
[179] P. Behroozi and J. Silk, The most massive galaxies and black holes allowed by ΛCDM, Mon. Not. R. Astron. Soc. **477**, 5382 (2018).
[180] H. Miyatake, Y. Harikane, M. Ouchi, Y. Ono, N. Yamamoto, A. J. Nishizawa, N. Bahcall, S. Miyazaki, and A. A. Plazas Malagón, First Identification of a CMB Lensing Signal Produced by 1.5 Million Galaxies at $z \sim 4$: Constraints on Matter Density Fluctuations at High Redshift, Phys. Rev. Lett. **129**, 061301 (2022).
[181] J. Evslin, Isolating the Lyman alpha forest BAO anomaly, J. Cosmol. Astropart. Phys. 04 (2017) 024.
[182] R. C. Bernardo, D. Grandón, J. Said Levi, and V. H. Cárdenas, Parametric and nonparametric methods hint dark energy evolution, Phys. Dark Universe **36**, 101017 (2022).
[183] N. Palanque-Delabrouille, C. Yèche, N. Schöneberg, J. Lesgourgues, M. Walther, S. Chabanier, and E. Armengaud, Hints, neutrino bounds and WDM constraints from SDSS DR14 Lyman-α and Planck full-survey data, J. Cosmol. Astropart. Phys. 04 (2020) 038.

[184] D. Valcin, J. L. Bernal, R. Jimenez, L. Verde, and B. D. Wandelt, Inferring the age of the universe with globular clusters, J. Cosmol. Astropart. Phys. 12 (2020) 002.

[185] J. L. Bernal, L. Verde, R. Jimenez, M. Kamionkowski, D. Valcin, and B. D. Wandelt, The trouble beyond H_0 and the new cosmic triangles, Phys. Rev. D **103**, 103533 (2021).

[186] S. Vagnozzi, F. Pacucci, and A. Loeb, Implications for the Hubble tension from the ages of the oldest astrophysical objects, J. High Energy Astrophys. **36**, 27 (2022).

[187] R. J. Cooke, M. Pettini, and C. C. Steidel, One percent determination of the primordial deuterium abundance, Astrophys. J. **855**, 102 (2018).

[188] D. Scolnic, D. Brout, A. Carr, A. G. Riess, T. M. Davis, A. Dwomoh, D. O. Jones, N. Ali, P. Charvu, R. Chen *et al.*, The Pantheon + analysis: The full data set and light-curve release, Astrophys. J. **938**, 113 (2022).

[189] O. Akarsu, E. Di Valentino, L. A. Escamilla, S. Kumar, E. Ozulker, and J. A. Vazquez, Relaxing cosmological tensions with a sign switching cosmological constant: Curvature and $A_{\rm lens}$ anomalies (to be published).